MIT NE 101

Fast Neutron Shielding Studies

by

Samuel Wilensky
Leon E. Beghian
Franklin Clikemann

Department of Nuclear Engineering
Massachusetts Institute of Technology
Cambridge, Massachusetts 02139

Supported by NASA Grant NsG-496

To the
National Aeronautics and Space Administration
Office of University Affairs

MIT NE 101

Fast Neutron Shielding Studies

by

Samuel Wilensky
Leon E. Beghian
Franklin Clikemann

Department of Nuclear Engineering
Massachusetts Institute of Technology
Cambridge, Massachusetts 02139

Supported by NASA Grant NsG-496

To the
National Aeronautics and Space Administration
Office of University Affairs

Table of Contents

	Page
List of Figures	i
A. Introduction	1
B. Fast Neutron Spectrometer	1
C. Calibration of the Spectrometer	3
D. Shielding Measurements	3
E. Time Dependent Neutron Spectrum Measurements	5
F. Conclusion	5
References	6

List of Figures

Figure 1 - Photomultiplier and Preamplifier

Figure 2 - Electronic Block Diagram

Figure 3 - Zero Crossing Time Spectrum

Figure 4 - Time-of-flight Neutron Spectra

Figure 5 - Recoil Proton Pulse Height Spectra

Figure 6 - Experimental Geometry

Figure 7a-n - Neutron Spectra from Iron-Paraffin Assemblies

Figure 8 - Time Spectrum from Iron Assembly

Figure 9a-f - Time Dependent Neutron Spectra from Iron Assembly

Shielding Properties of Iron and Paraffin Shields*

A. Introduction

The increased interest in the utilization of nuclear power for space application has introduced design problems which are not as important in stationary installations. One of the problems which is unique to the design of mobile nuclear power sources, particularly those which are to be flown, is weight consideration. The problem is to obtain the optimum configuration which will give the best shielding per unit weight. Shielding for gamma radiation and charged particles is straight forward in that a sufficient mass of material must be interposed to provide adequate shielding. For neutrons, particularly fast neutrons, the shielding problem is much more complex. Materials with a high non-elastic scattering cross section, such as iron, are excellent for degrading the energy of fast neutrons, but are ineffective as moderators of neutrons of intermediate energy. Likewise hydrogenous material such as paraffin are very efficient for moderating intermediate and low energy neutrons, but are not as effective in degrading fast neutrons.

The work described below describes a neutron spectroscopy technique which has been used to study the shielding properties of iron-paraffin assemblies. The spectrometer has also been used to measure time dependent neutron spectra from an iron assembly after excitation by a pulse of mono-energetic neutrons.

B. Fast Neutron Spectrometer

The experimental measurement of the shielding properties of materials for fast neutrons necessitates an instrument capable of measuring fast neutron spectra with good energy resolution, high efficiency and low sensitivity to gamma radiation. Of the numerous neutron spectroscopy techniques available the only technique which has sufficient efficiency and energy resolution is the proton recoil scintillation spectrometer. The detector used for this work was a 1" diameter x 1" thick stilbene scintillator coupled to an RCA 7264 photomultiplier. The principle of operation of the proton recoil scintillation spectrometer has been described in Reference 1. Although the sensitivity and resolution of this detector is adequate, it does have a high sensitivity for gamma radiation. Fortunately pulses produced by neutrons (recoil protons) can be distinguished from gamma radiation (Compton electrons) by detecting the difference in their pulse shape.

Gamma radiation discrimination circuits depend on detecting the difference in the rise times of the pulses due to recoil protons and those caused by Compton electrons. If the linear signal from the photomultiplier is doubly differentiated, the time between the beginning of the pulse and the first zero crossing will depend on the rise time of the pulse. This time difference can be measured and will indicate whether an event is a recoil proton or a Compton electron.

The preamplifier and resistor bleeder network used with the RCA 7264 is shown in Figure 1. The preamplifier provides two outputs. A fast output (from the anode) which is used to generate the time mark for the beginning

---

* This work was supported by NASA Grant NsG-496

of the scintillation pulse, and a slow or linear signal which is taken off the last dynode. A 47 μf capacitor has been added between the last dynode and ground to increase the decay time of the linear pulse to approximately 50 μs. The addition of the capacitor allows the double differentiation to be accomplished at a latter stage of amplification.

A block diagram of the gamma discrimination, timing and spectroscopy electronics is shown in Figure 2. The pulse shape discriminator or "n,γ" channel operates in the following manner. The leading edge of the fast output of the photomultiplier is detected by an ORTEC 260 and ORTEC 403 tunnel diode discriminator. The trigger level of the tunnel diode discriminator was adjusted to just eliminate the thermal noise from the photomultiplier photocathode. The slow output from the photomultiplier is amplified and doubly differentiated (double delay line) by an ORTEC 410. The double delay line differentiated output from the ORTEC 410 is fed to an ORTEC 407 zero crossing detector. The output from the zero crossing detector is used to strobe an ORTEC 404 single channel analyzer which has been conditioned by the singularly differentiated pulse from the ORTEC 410. The level of the single channel analyzer is set to eliminate low energy noise. The time difference between the start of the photomultiplier pulse (output of ORTEC 403) and the zero crossing of the doubly differentiated pulse is determined by an EG & G time-to-amplitude converter. A delay has been inserted between ORTEC 403 and the EG & G to subtract a fixed "bias" from the output of the time-to-amplitude converter. *

The time channel which was used in conjunction with pulsed Van der Graaf accelerator to calibrate the spectrometer is described in Reference 1. In concept, the only difference in the electronics described in this reference and the present electronic circuits used for these measurements is the addition of the "n,γ" channel which discriminates against gamma radiation.

Using a remote switching system activated from the accelerator control room it was possible to record the following spectra.

(1) Time-of-flight neutron spectra (Fig. 4)

(2) Recoil proton pulse height spectra (Fig. 5)

(3) Zero crossing time spectrum (Fig. 3)

Each of the above spectra could be gated by its own signal which facilitates setting the "n,γ" and time-of-flight window. Provisions are included for recording any of the three spectra gated by the other two. For example a Recoil pulse height spectrum which resulted from events occurring at a selected time interval after the accelerator pulse and which has a preselected zero crossing time could be recorded.

---

* The output of the time-to-amplitude converter is used to drive a single channel analyzer (SCA) whose output is used to select neutron events and reject events from gamma radiation. A typical "n,γ" time spectrum is shown in Figure 3.

C. Calibration of the Spectrometer

A detailed description of the calibration procedure is given in Reference 1, but a summary of the technique is presented below for convenience.

The utilization of a recoil proton scintillation spectrometer necessitates the unfolding of the proton recoil spectrum to obtain the neutron spectrum. The mathematical technique for the unfolding or deconvolution used for this work was formulated by W. R. Burrus and is described in Reference 2. A necessary input to the unfolding code (FERDO) is the response of the proton recoil spectrometer to monoenergetic neutrons. The response functions were measured by placing the detector $\sim$ 50 cm from the accelerator target. The accelerator used was a pulsed Van der Graaf machine capable of accelerating protons of energies between 1.4 and 3.1 MeV. The neutron producing target was a 40 KeV thick tritum target which gave monoenergetic neutron beams between 200 KeV and 2.2 MeV. For measurement of the response functions the accelerator was run in a pulsed mode and a time window used to select only those neutrons which arrived at the detector at the proper time after the accelerator pulse. A typical detector spectrum from monoenergetic neutrons is shown in Figure 5. Each monoenergetic response function was normalized using a BF_3 detector which has been shown to have a uniform response for neutrons of energies between 200 KeV and 3.0 MeV.

D. Shielding Measurements

The purpose of this investigation was to measure the neutron energy spectrum transmitted through a shield wall for a given energy of an incident monoenergetic neutron beam. The geometry for the shielding measurements is shown in Figure 6. The distance between the accelerator and the detector was maintained at 75 cm. The rear face of shield wall was always placed near the detector and layers of shielding material were added to bring the front face of the wall nearer to the accelerator target. Each layer of material was 18" high and 18" wide. The iron layers were 6" thick and the paraffin layers 5" thick. A continuous monoenergetic neutron beam (1.9 ± 0.03 MeV) neutron beam was incident on the front surface of the shielding assembly. The transmitted neutron energy spectrum was determined for a variety of shield configurations. Additional calculations of relative transmission, average energy and relative biological dose were also made. The relative transmission is defined as the faction of neutrons reaching the detector with the shield in place as compared to the number of neutrons reaching the detector with no shield. The relative dose is defined as the faction of dose received with present as compared to the dose received with no shield. The calculation of the relative number of neutrons in the spectrum, the average neutron energy and the relative dose are performed as an integral part of the FERDO unfolding code. As described in Reference 1 the unfolding code (formally known as SLOP) publishes not only the neutron spectrum, but also the integral of the neutron spectrum folded with any arbitrary function. If a flat function is selected, the integral

$$N = \int_{E_{min}}^{E_{max}} \Phi(E)\, dE$$

will be proportional to the number of neutrons in the spectrum (E) between the energy limits E_{max} and E_{min}. If a linear ramp is chosen as the function the integral

$$M = \int_{E_{min}}^{E_{max}} E \cdot \phi (E) d E$$

will be proportional to the first moment of the energy spectra. To obtain the average energy (E) one divides M by N.

$$\overline{E} = \frac{M}{N} = \frac{\int_{E_{min}}^{E_{max}} E \cdot \phi (E) d E}{\int_{E_{min}}^{E_{max}} \phi (E) d E}$$

The relative dose can be calculated in a similar manner using the relative biological response B (E) as the function which is folded with energy spectrum to obtain the relative dose.

$$\text{Relative Dose} = \int_{E_{min}}^{E_{max}} B(E) \cdot \phi (E) d E$$

The biological response B (E) was obtained from Reference 3 and is listed below.

Neutron Energy (MeV)	Relative Biological Effect
0.1	1/250
0.5	1/90
1.0	1/60
2.5	1/60

The intermediate energies were obtained by linear interpolation.

The relative number of neutrons, the average energy and the relative biological dose for a number of iron-paraffin walls are given in Table 1. The first column of the table is the run identification number, the second column the relative number of neutrons, the third column the average energy, the fourth column the relative dose and the last column indicates the geometry and composition of the shielding wall. For example Run 71 consisted of a 6" thick wall of iron facing the neutron source, a 6" thick wall of iron behind that and a 5" thick wall of paraffin next to the detector. Run 60 was made with no wall in place and results from this run were used to normalize all the other results.

The neutron spectra obtained from each run are shown in Figure 7a-n. Run 65 and 66, two runs which were made under the same conditions, yielded results which were within the uncertainty of the measurements.

It should be noted that in all cases where the iron is placed in the front of the shielding wall and the paraffin on the rear of the shielding wall the dose is less than that obtained with the reverse configuration (for example Run 71 as compared to Run 69). This result can be attributed to the large nonelastic cross-section of iron which degrades the high energy neutrons and strong moderating property of paraffin for low energy neutrons. In the reverse case the paraffin has a much smaller cross section for fast neutrons and as a result is less effective when placed at the front and the large mass of the iron nucleus makes it ineffectual for moderating neutrons of energy less than 845 KeV, the first excited level for Fe^{56}.

E. Time Dependent Neutron Spectrum Measurements

The speed of response of the recoil proton scintillation spectrometer makes it possible to measure the time dependence of the neutron spectrum emerging from an iron assembly after the injection of a short burst of mono-energetic neutrons.

To demonstrate the feasibility of the spectrometer for making this type of measurement short pulses ($\sim$5 ns) of 2 MeV neutrons were injected into a 18" x 18" x 6" iron assembly. The time decay curve shown in Figure 8 was measured with the detector biased to accept all neutrons above 200 KeV. Energy spectrum were then recorded for the time windows indicated on Figure 8. The time window on the left gave the background spectrum, the next time window to the right gave the spectrum just after the primary pulse entered the assembly and the other time windows give the spectra at times correspondingly further away in time from the initial pulse. The data in each time window were normalized with a BF_3 counter in a fashion similar to the shielding studies. The background measurement was subtracted from the other runs before the data was unfolded with FERDO. The background was assumed to be time independent since the period of the pulsed accelerator (125 ns) was much greater than the slowing down time of neutrons and a pseudo equilibrium spectrum is established. The unfolded results are shown in Figures 9a-k. The first time interval (Run 82) indicates two peaks; a primary peak at the energy of the initial pulse and a second peak approximately 850 KeV below the energy of the initial peak. The second peak is due to the large, inelastic scattering at the first excited level of Fe^{56} (845 KeV). Run 85 depicts the spectrum a little further on in time and shows the small peak of Run 82 growing and the large peak decreasing as the neutrons are degraded in energy. Further along in time (Run 87, 89, 91, 93) the high energy peak disappears and the low energy peak spreads and degrades with time. This illustrates the degration of neutron energy with time spent in the assembly, caused by multiple scattering.

F. Conclusion

It has been shown that quantitative fast neutron shielding measurements can be made with a proton recoil scintillation spectrometer. The technique could be very valuable in verifying theoretical shielding calculations in simple geometry which could later be applied to more complex geometries. The proton recoil scintillation spectrometer has also been shown to be a useful tool in measuring time dependent neutron spectra. These results would be useful in verifying results from theoretical calculations of fast reactor kinetics.

References

1. L. E. Beghian, S. Wilensky and W. R. Burrus; A Fast Neutron Spectrometer Capable of Manosecond Time Gating; Nuclear Instruments and Methods 35 (1965) 34-44.

2. W. R. Burrus, Ph.D. Thesis; Ohio State University, Columbus, Ohio (1964); also ORNL-3743.

3. H. Etherington, Nuclear Engineering Handbook, McGraw-Hill Book Company, New York (1958) 7-84.

Table 1

Run	Number (Relative)	Energy (MeV)	Dose (Relative)	Beam
60	1.000 ± 0.050	1.640 ± 0.097	1.000 ± 0.039	-
61	$.296 \pm 0.028$	$.946 \pm 0.111$	$.255 \pm 0.063$	Fe
63	$.353 \pm 0.040$	$.618 \pm 0.107$	$.260 \pm 0.085$	FeFe
65	$.195 \pm 0.028$	$.532 \pm 0.108$	$.133 \pm 0.098$	FeFeFe
66	$.181 \pm 0.025$	$.525 \pm 0.122$	$.123 \pm 0.113$	FeFeFe
69	$.059 \pm 0.010$	$.677 \pm 0.181$	$.046 \pm 0.125$	FeFePa
70	$.054 \pm 0.006$	$.583 \pm 0.102$	$.040 \pm 0.085$	FePaFe
71	$.045 \pm 0.004$	$.576 \pm 0.093$	$.032 \pm 0.080$	PaFeFe
72	$.037 \pm 0.004$	$.621 \pm 0.105$	$.028 \pm 0.082$	PaFePa
73	$.033 \pm 0.005$	$.659 \pm 0.137$	$.026 \pm 0.098$	PaPaFe
74	$.072 \pm 0.006$	$.662 \pm 0.074$	$.055 \pm 0.062$	PaPa
75	$.044 \pm 0.005$	$.631 \pm 0.115$	$.033 \pm 0.090$	PaPaPa
76	$.266 \pm 0.018$	$.922 \pm 0.077$	$.224 \pm 0.050$	Pa
77	$.047 \pm 0.007$	$.645 \pm 0.102$	$.036 \pm 0.073$	FePaPa

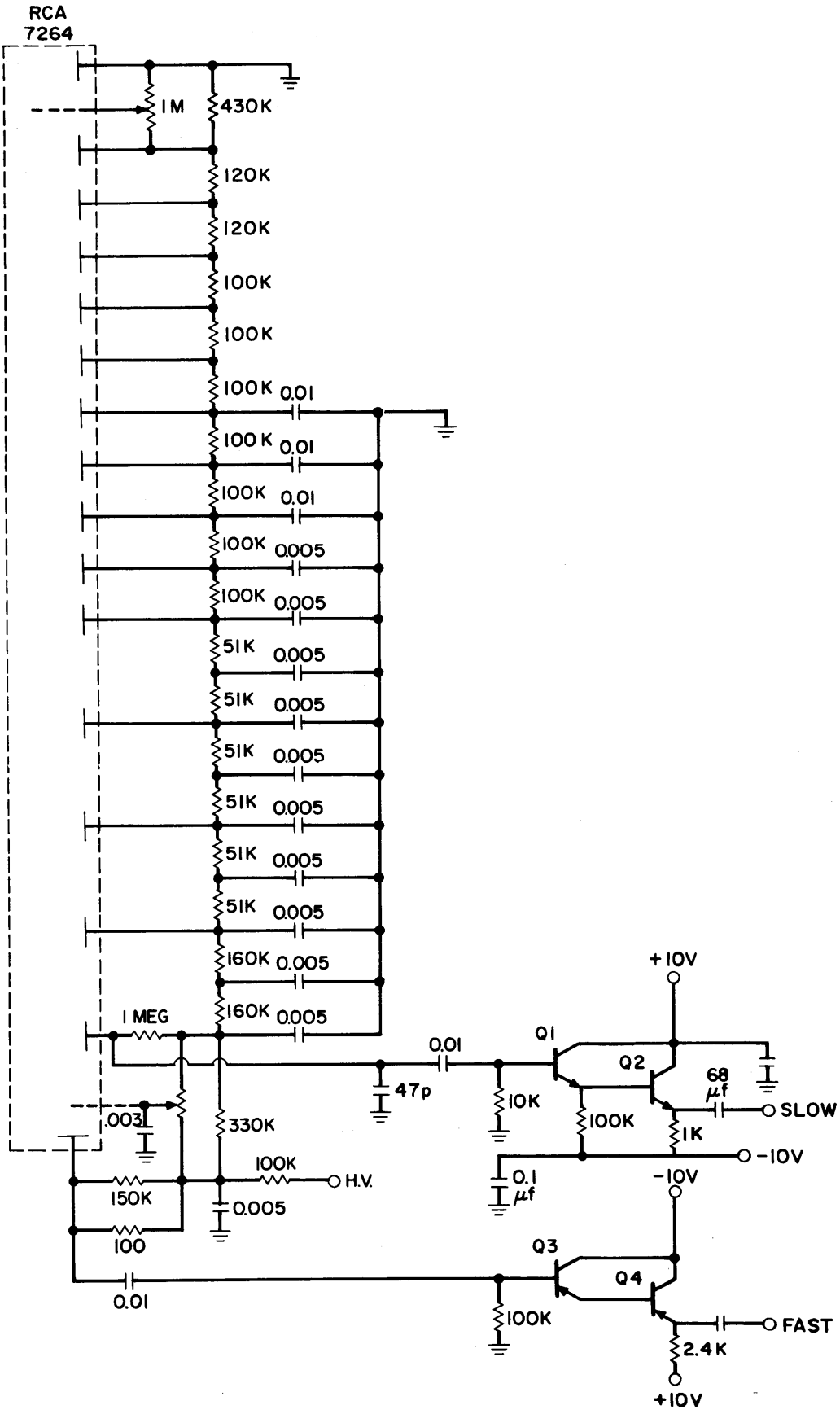

figure 1 - Photomultiplier and Preamplifier

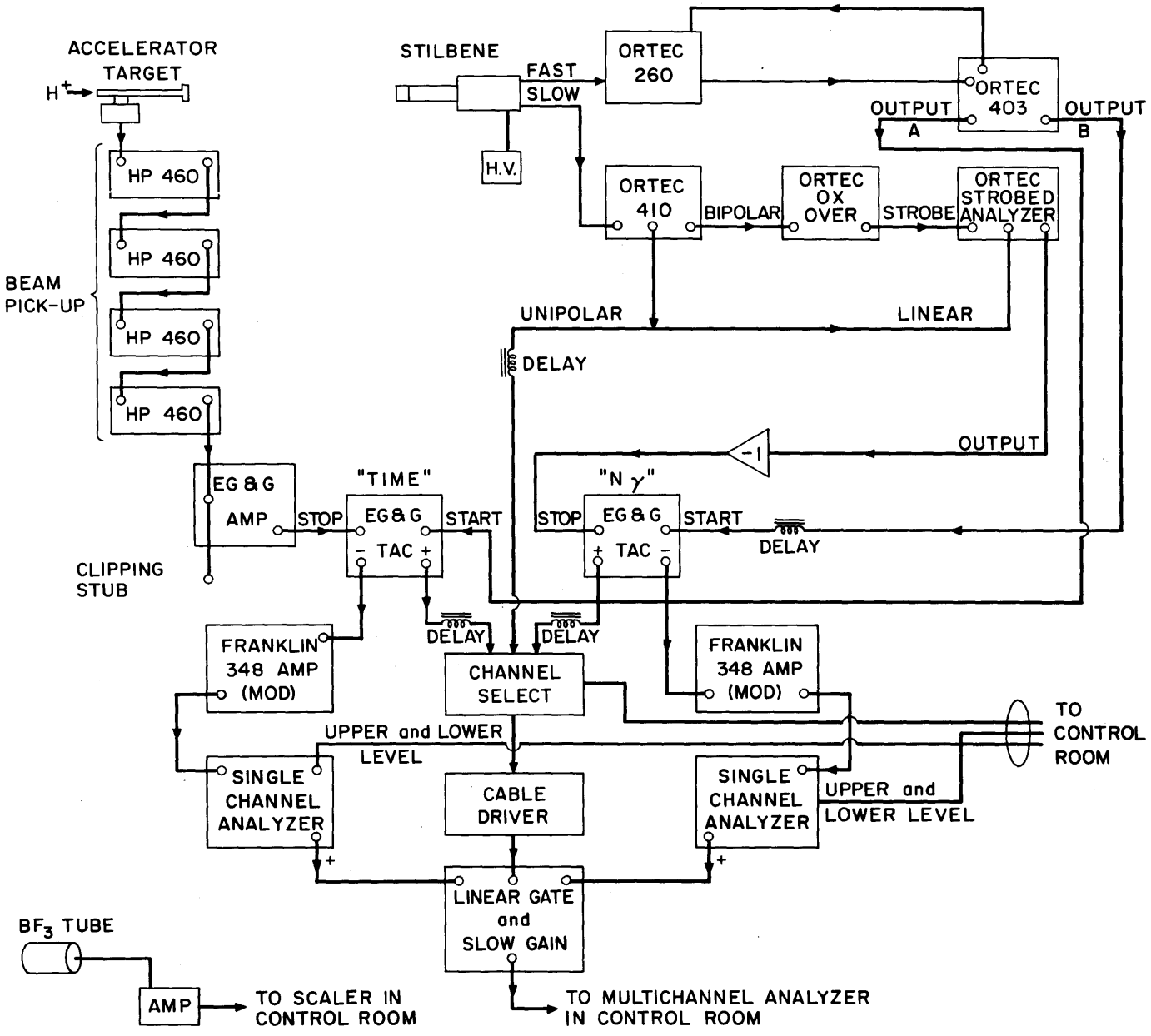

figure 2 - Electric Block Diagram

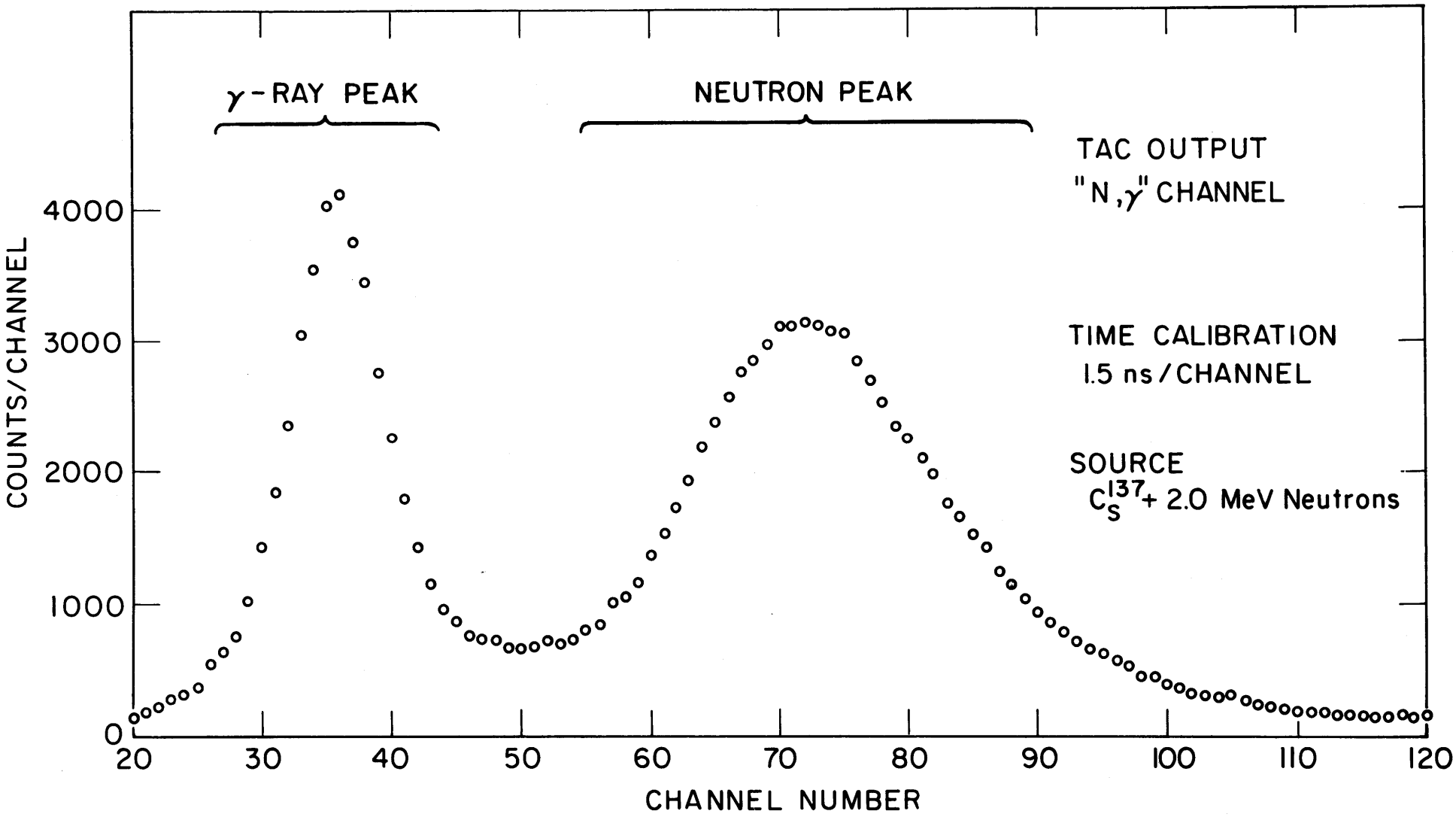

figure 3 - Zero Crossing
Time Spectrum

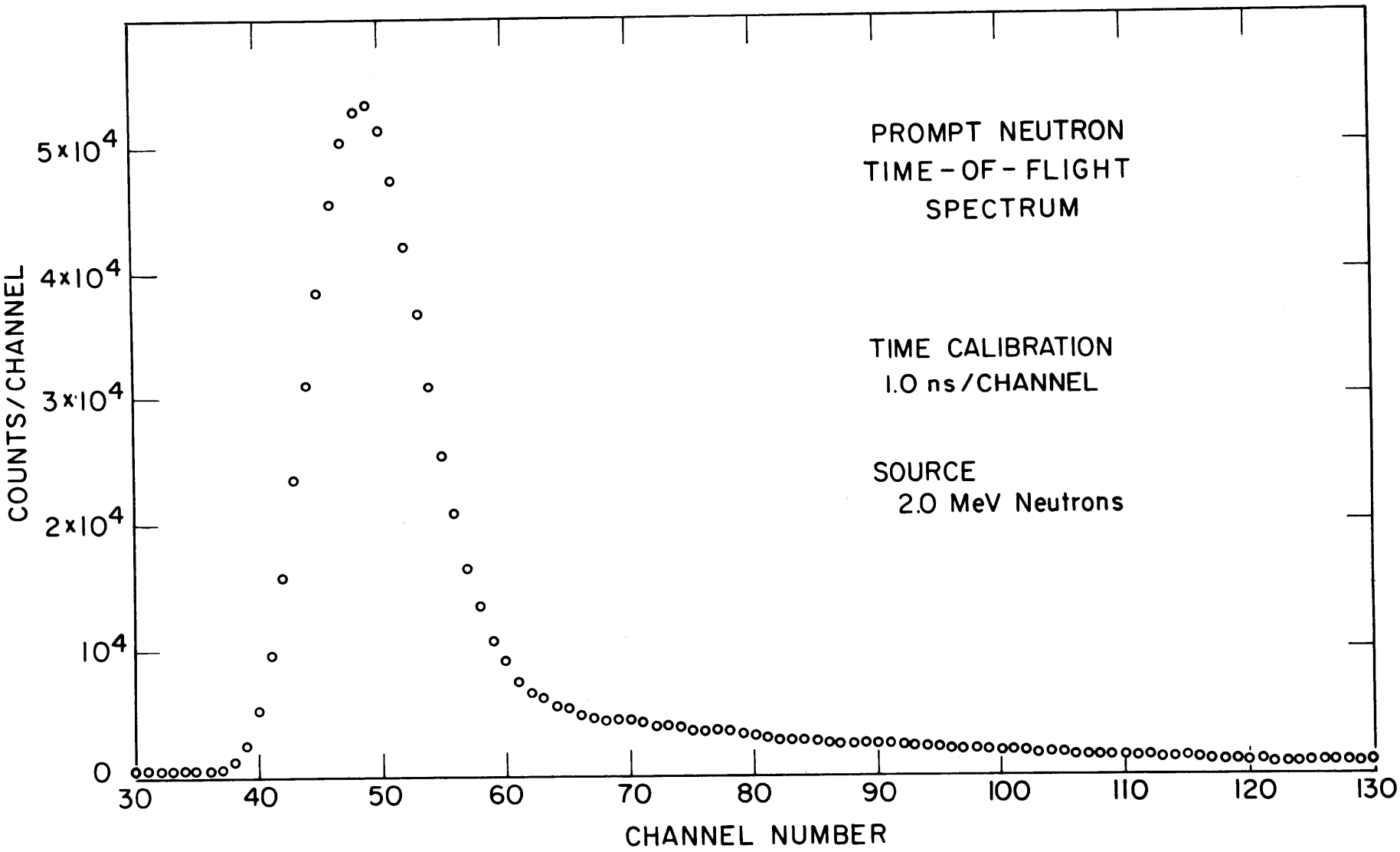

figure 4 - Time-of-flight
Neutron Spectrum

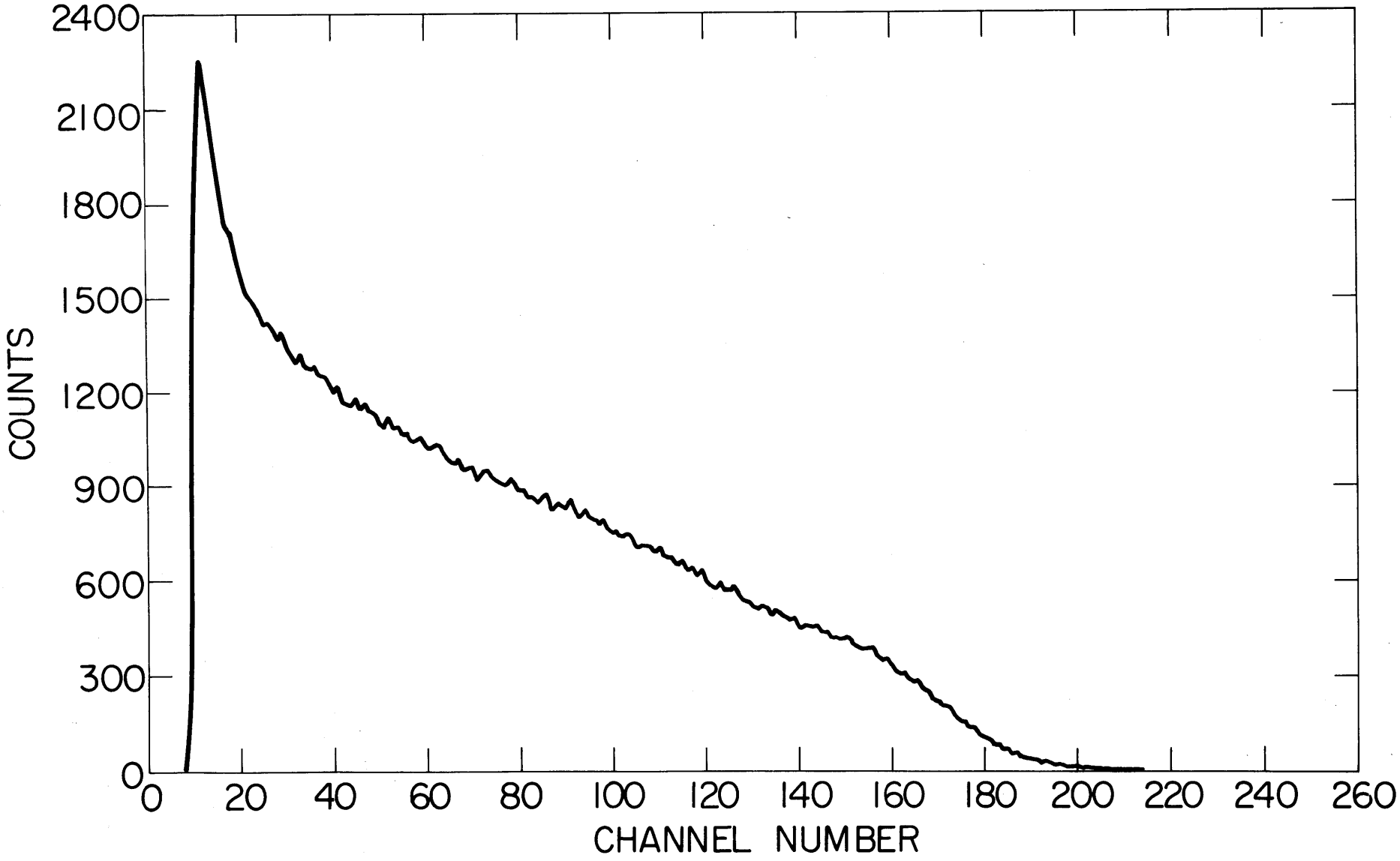

figure 5 - Recoil Proton Pulse Height Spectrum

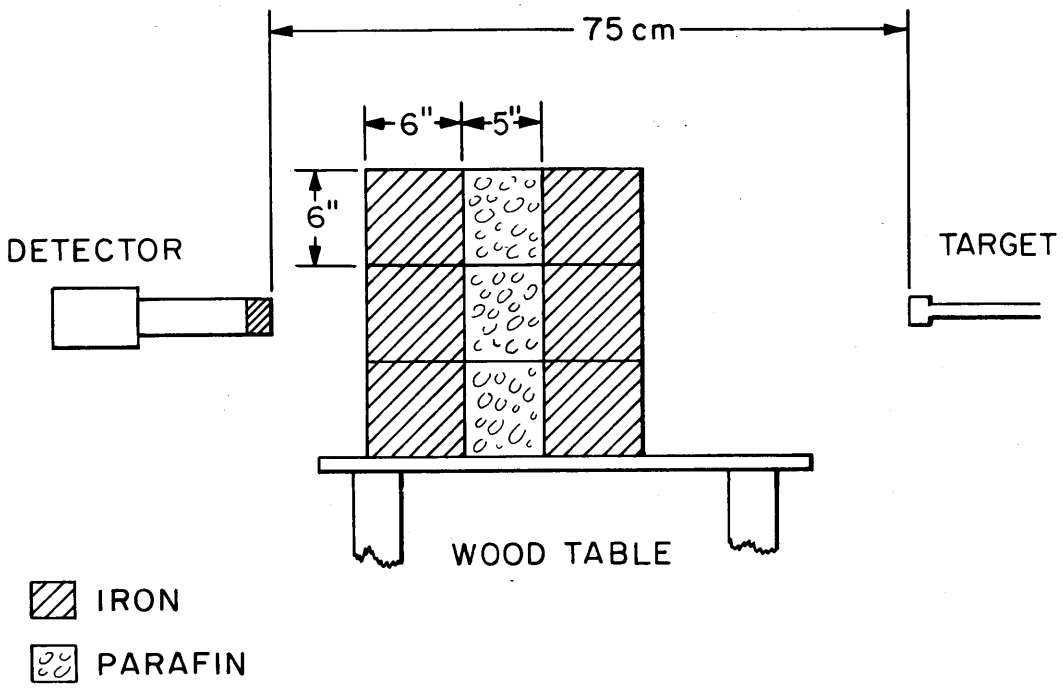

figure 6 - Experimental Geometry

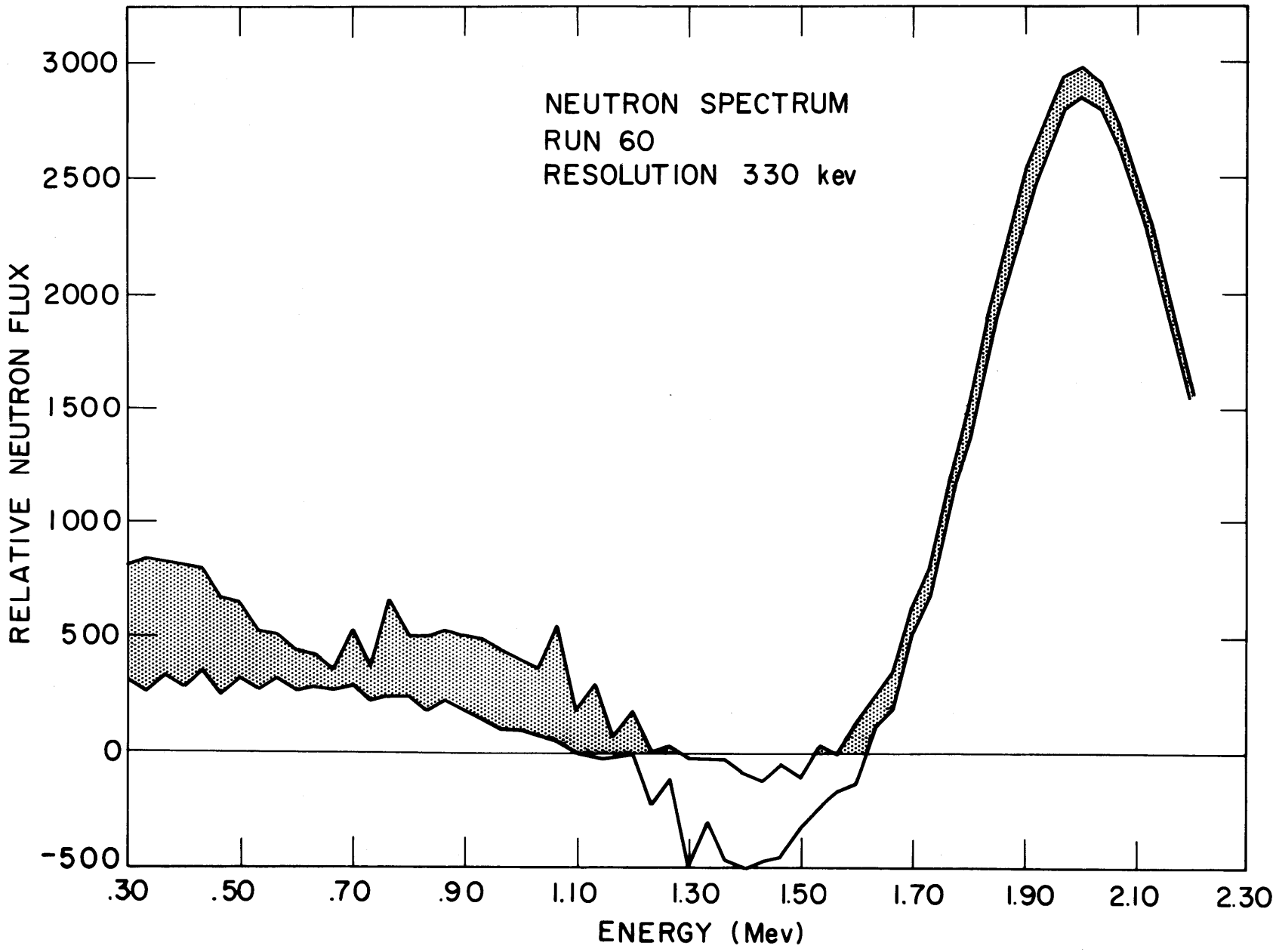
NEUTRON SPECTRUM
RUN 60
RESOLUTION 330 kev
RELATIVE NEUTRON FLUX
3000
2500
2000
1500
1000
500
0
-500
.30
.50
.70
.90
1.10
1.30
1.50
1.70
1.90
2.10
2.30
ENERGY (Mev)

figure 7_a

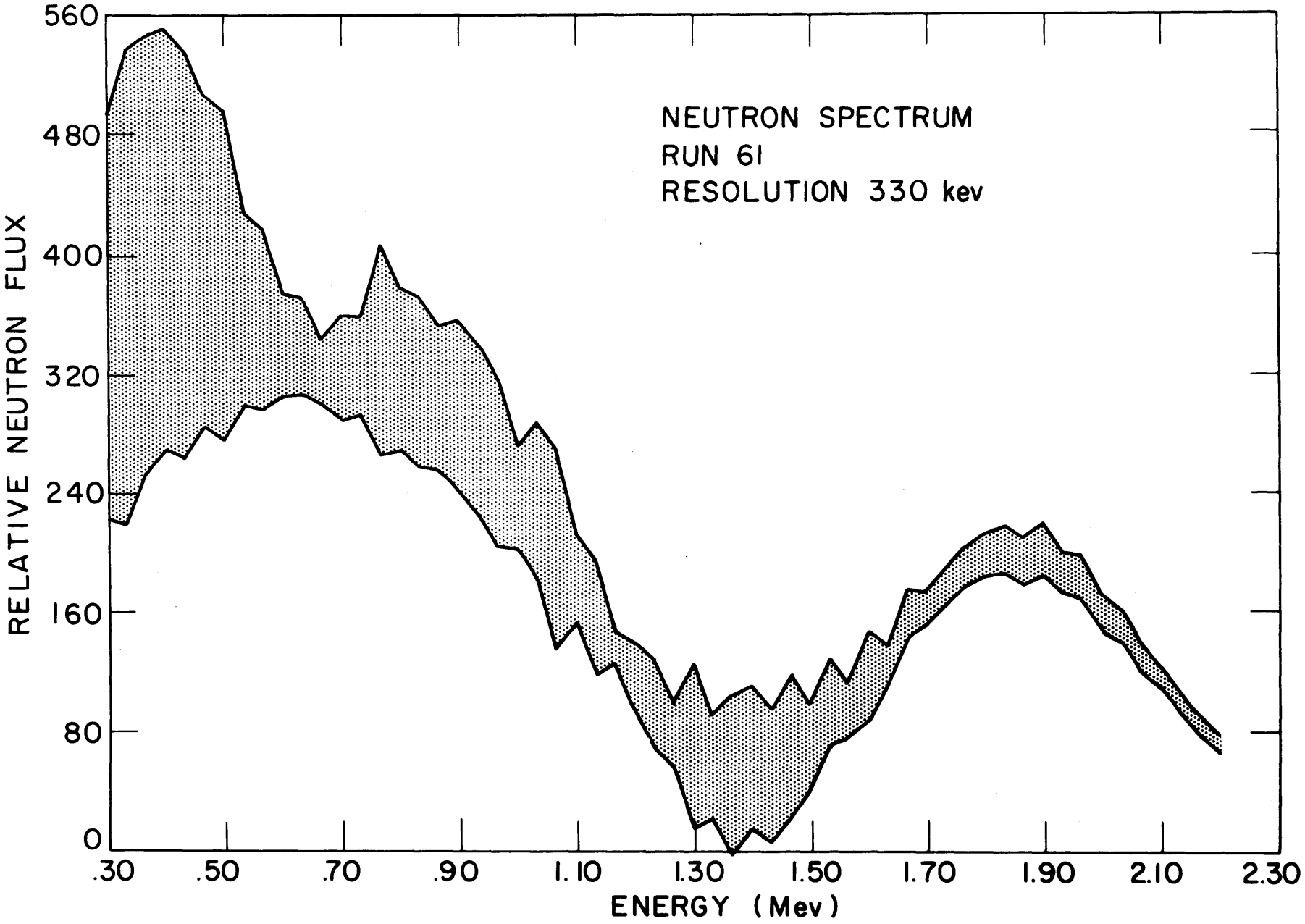
NEUTRON SPECTRUM
RUN 61
RESOLUTION 330 kev
RELATIVE NEUTRON FLUX
560
480
400
320
240
160
80
0
.30
.50
.70
.90
1.10
1.30
1.50
1.70
1.90
2.10
2.30
ENERGY (Mev)

figure 7_b

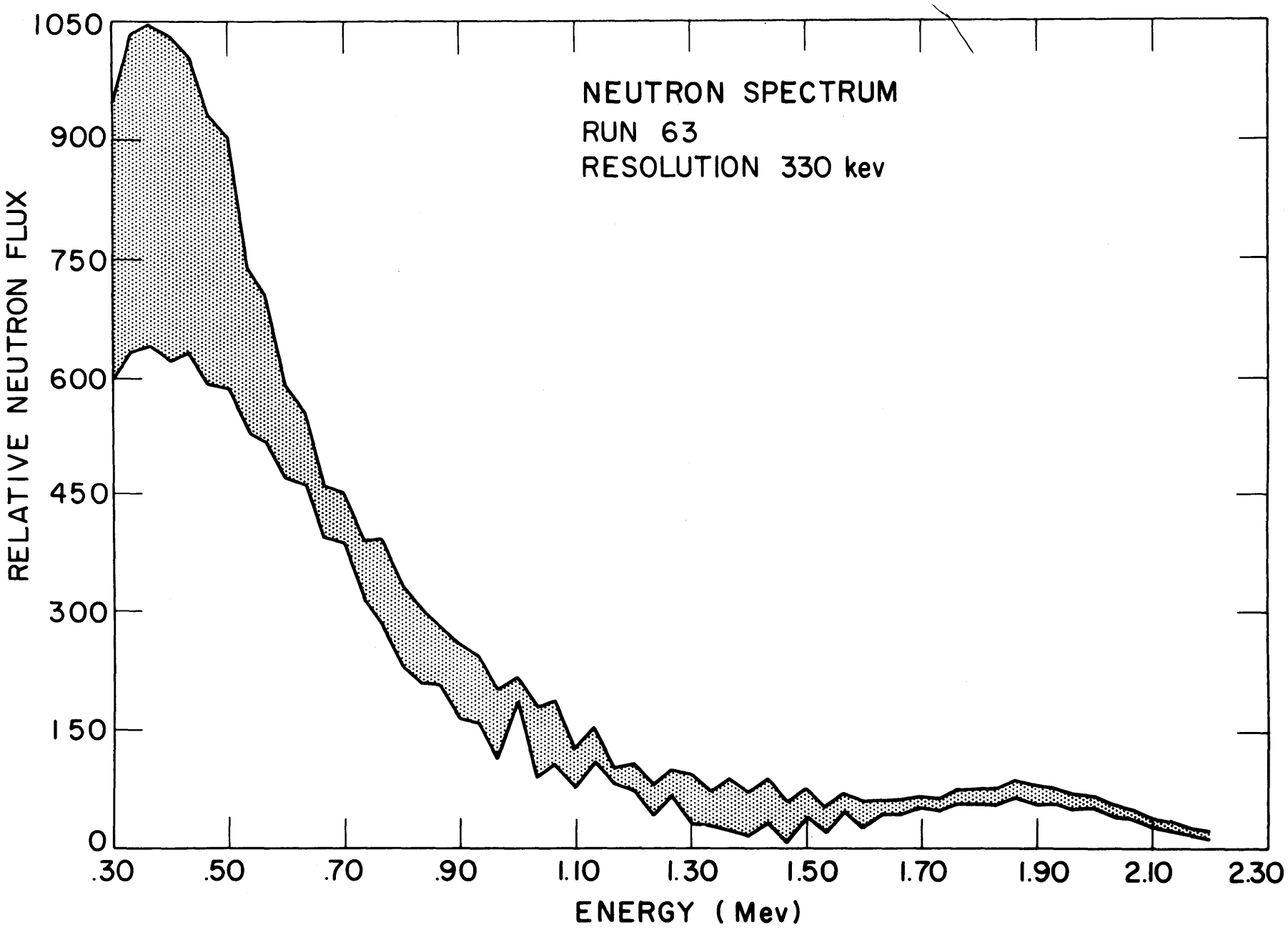
NEUTRON SPECTRUM
RUN 63
RESOLUTION 330 kev
RELATIVE NEUTRON FLUX
1050
900
750
600
450
300
150
0
.30
.50
.70
.90
1.10
1.30
1.50
1.70
1.90
2.10
2.30
ENERGY (Mev)

figure 7_c

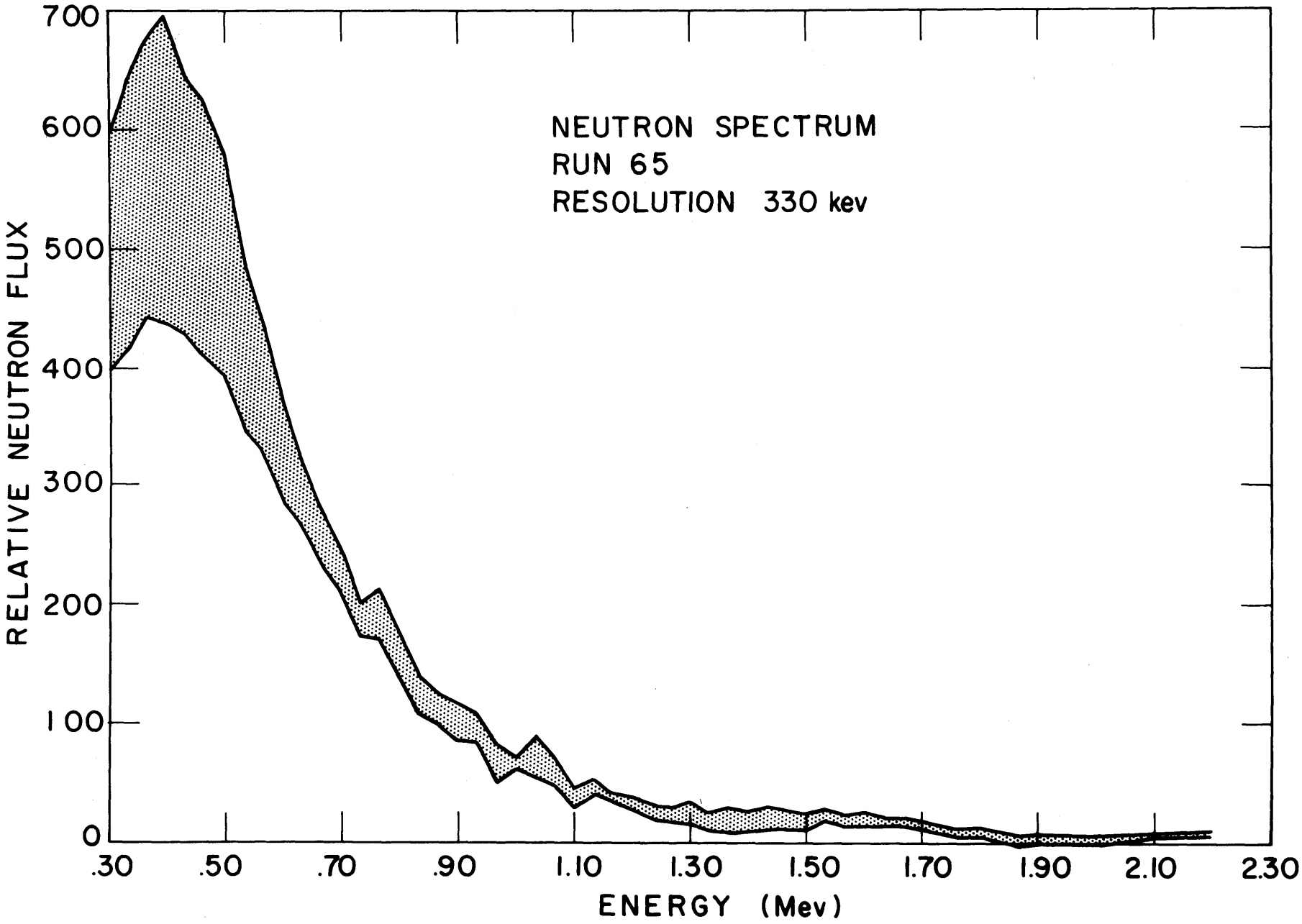
NEUTRON SPECTRUM
RUN 65
RESOLUTION 330 kev
RELATIVE NEUTRON FLUX
700
600
500
400
300
200
100
0
.30
.50
.70
.90
1.10
1.30
1.50
1.70
1.90
2.10
2.30
ENERGY (Mev)

figure 7_d

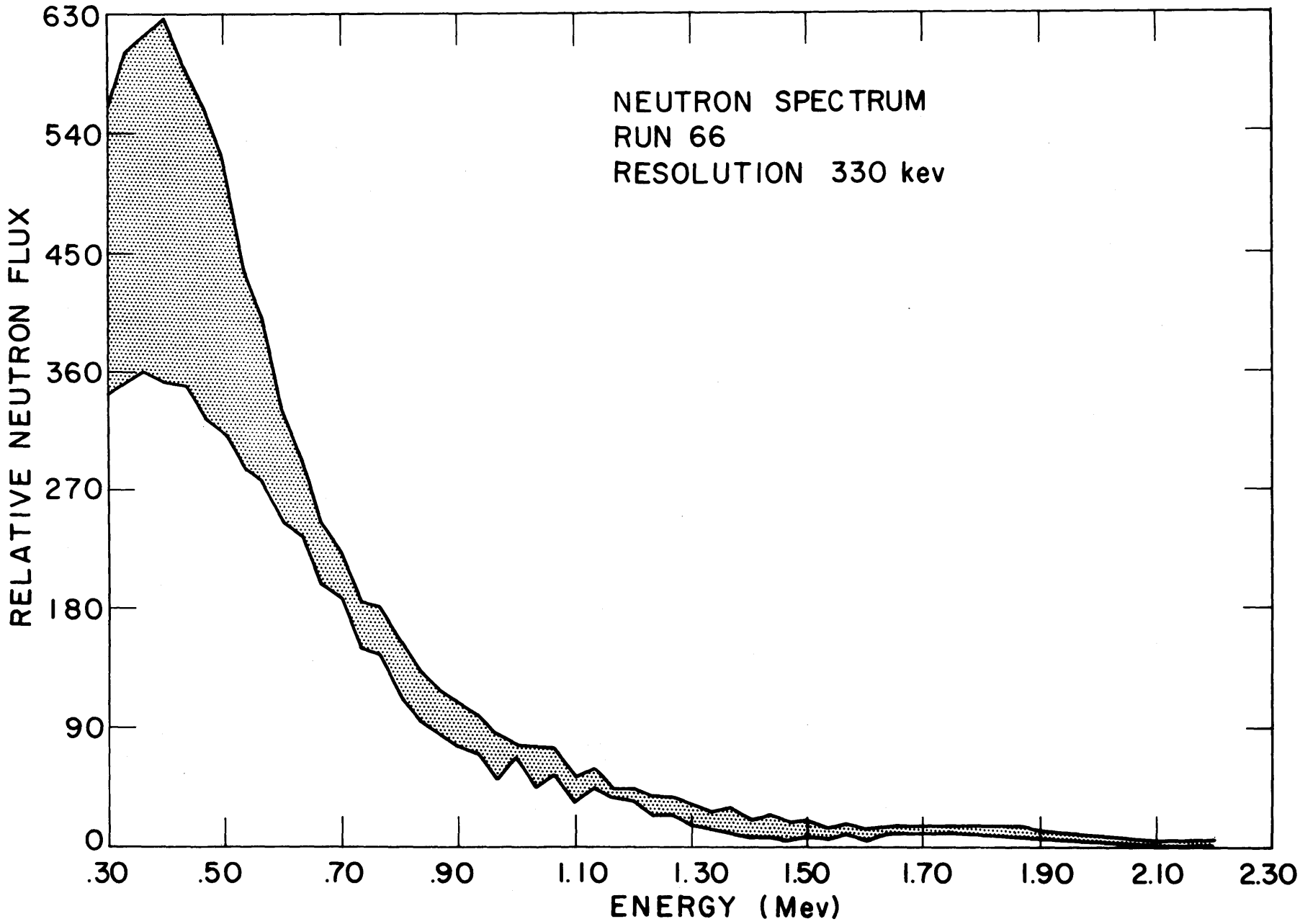
NEUTRON SPECTRUM
RUN 66
RESOLUTION 330 kev
RELATIVE NEUTRON FLUX
630
540
450
360
270
180
90
0
.30
.50
.70
.90
1.10
1.30
1.50
1.70
1.90
2.10
2.30
ENERGY (Mev)

figure 7$_e$

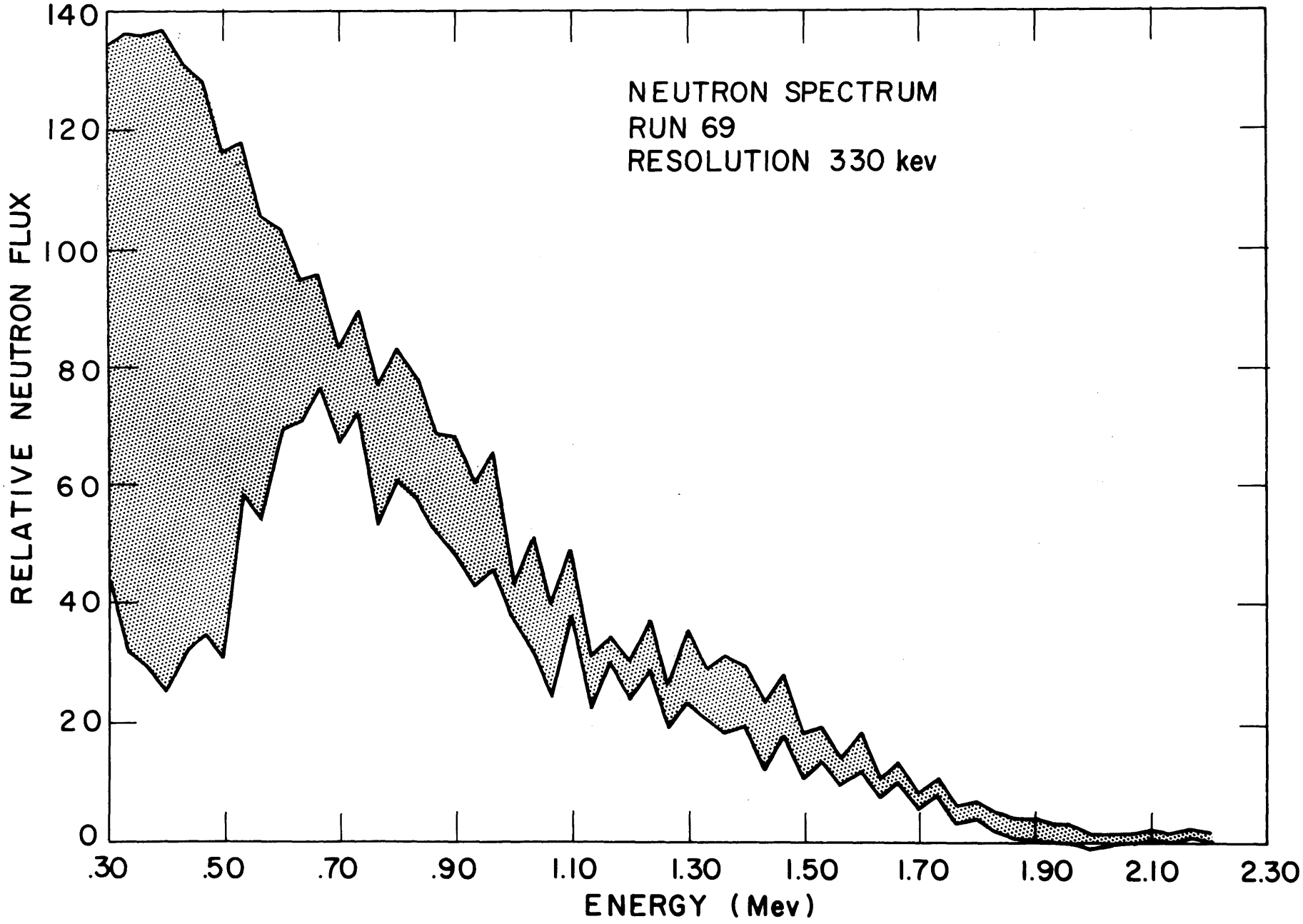
NEUTRON SPECTRUM
RUN 69
RESOLUTION 330 kev
RELATIVE NEUTRON FLUX
140
120
100
80
60
40
20
0
.30
.50
.70
.90
1.10
1.30
1.50
1.70
1.90
2.10
2.30
ENERGY (Mev)

figure 7_f

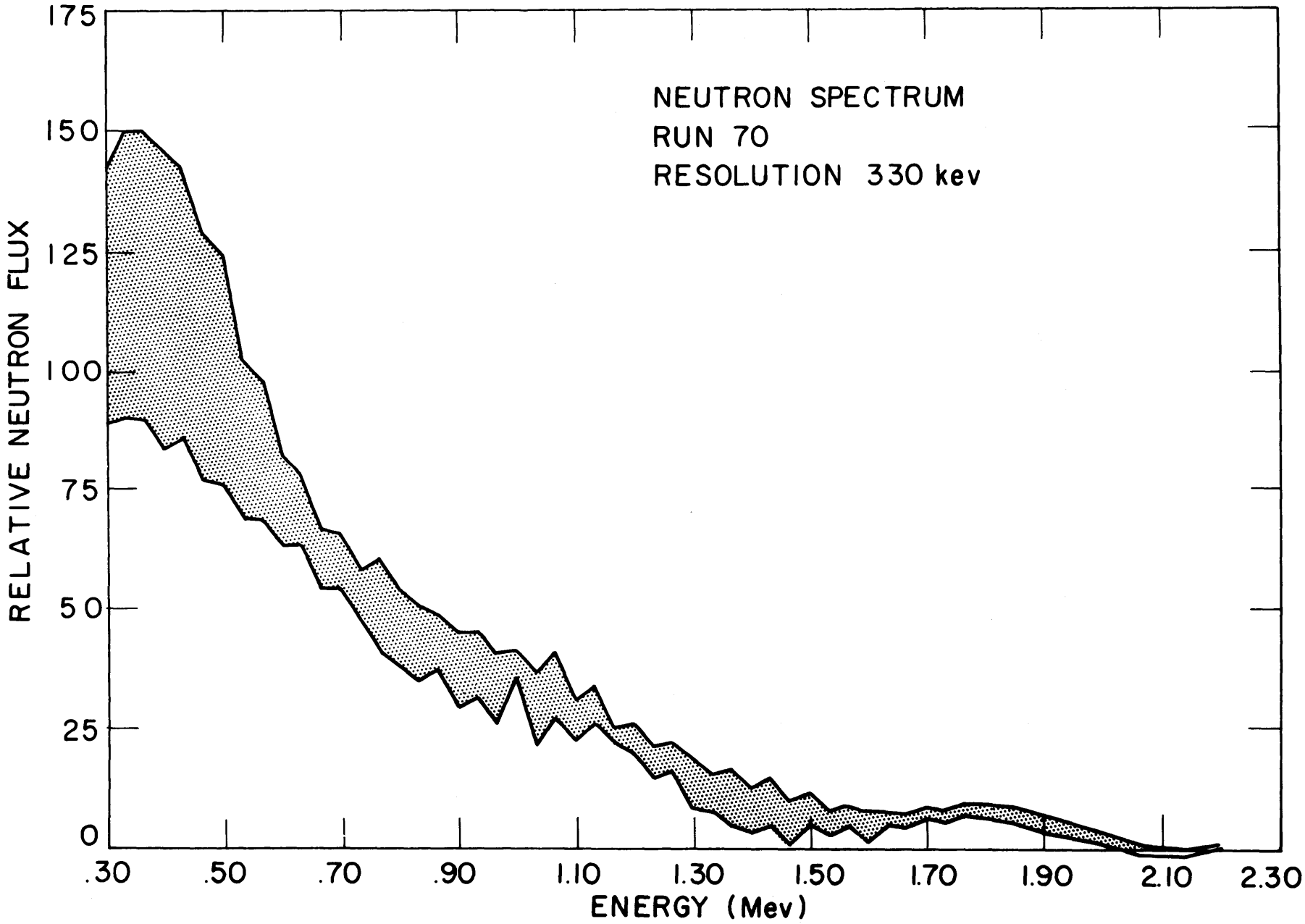
NEUTRON SPECTRUM
RUN 70
RESOLUTION 330 kev
RELATIVE NEUTRON FLUX
175
150
125
100
75
50
25
0
.30
.50
.70
.90
1.10
1.30
1.50
1.70
1.90
2.10
2.30
ENERGY (Mev)

figure 7g

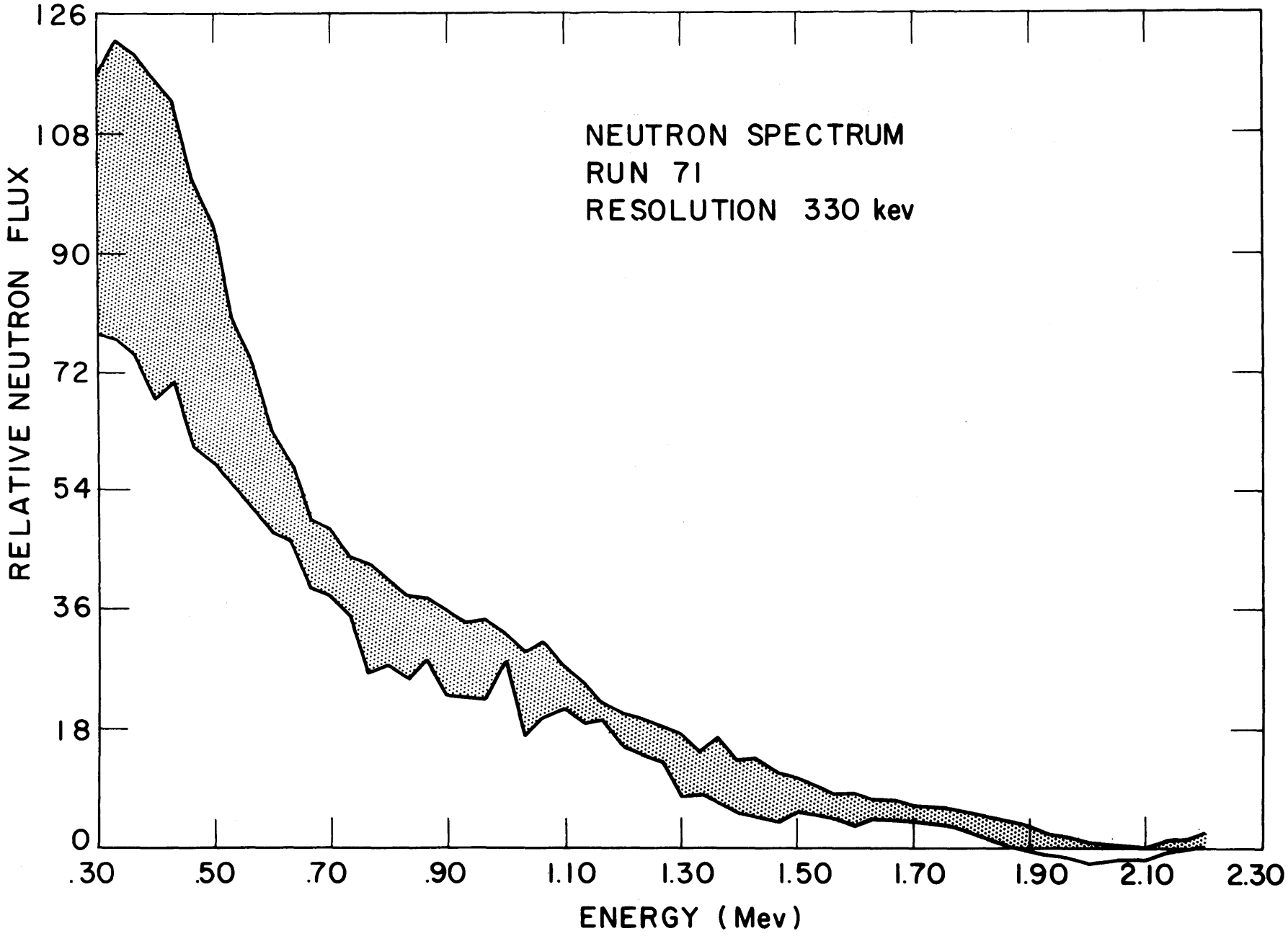
NEUTRON SPECTRUM
RUN 71
RESOLUTION 330 kev
RELATIVE NEUTRON FLUX
126
108
90
72
54
36
18
0
.30
.50
.70
.90
1.10
1.30
1.50
1.70
1.90
2.10
2.30
ENERGY (Mev)

figure 7_h

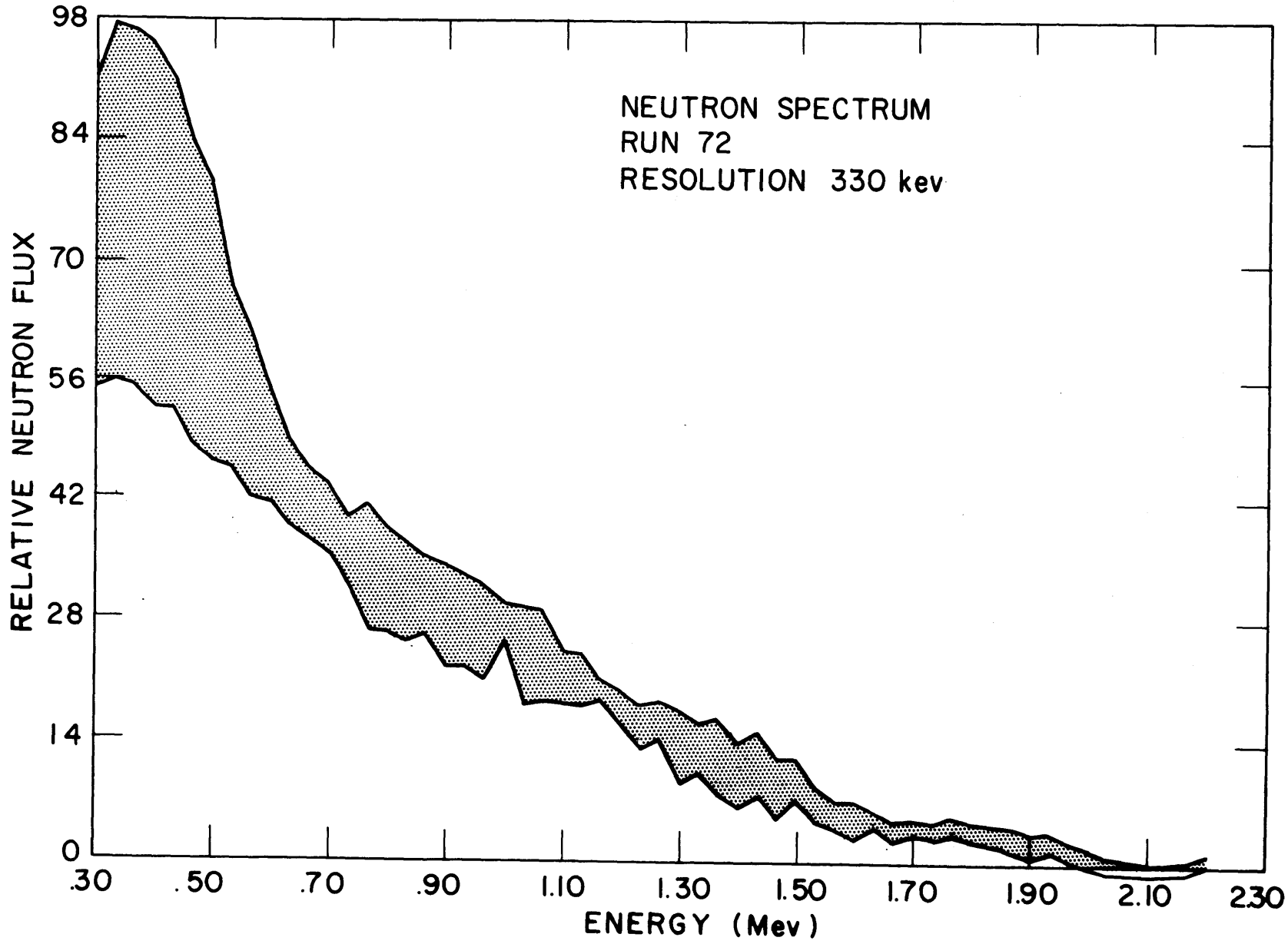
NEUTRON SPECTRUM
RUN 72
RESOLUTION 330 kev
RELATIVE NEUTRON FLUX
98
84
70
56
42
28
14
0
.30
.50
.70
.90
1.10
1.30
1.50
1.70
1.90
2.10
2.30
ENERGY (Mev)

figure 7_i

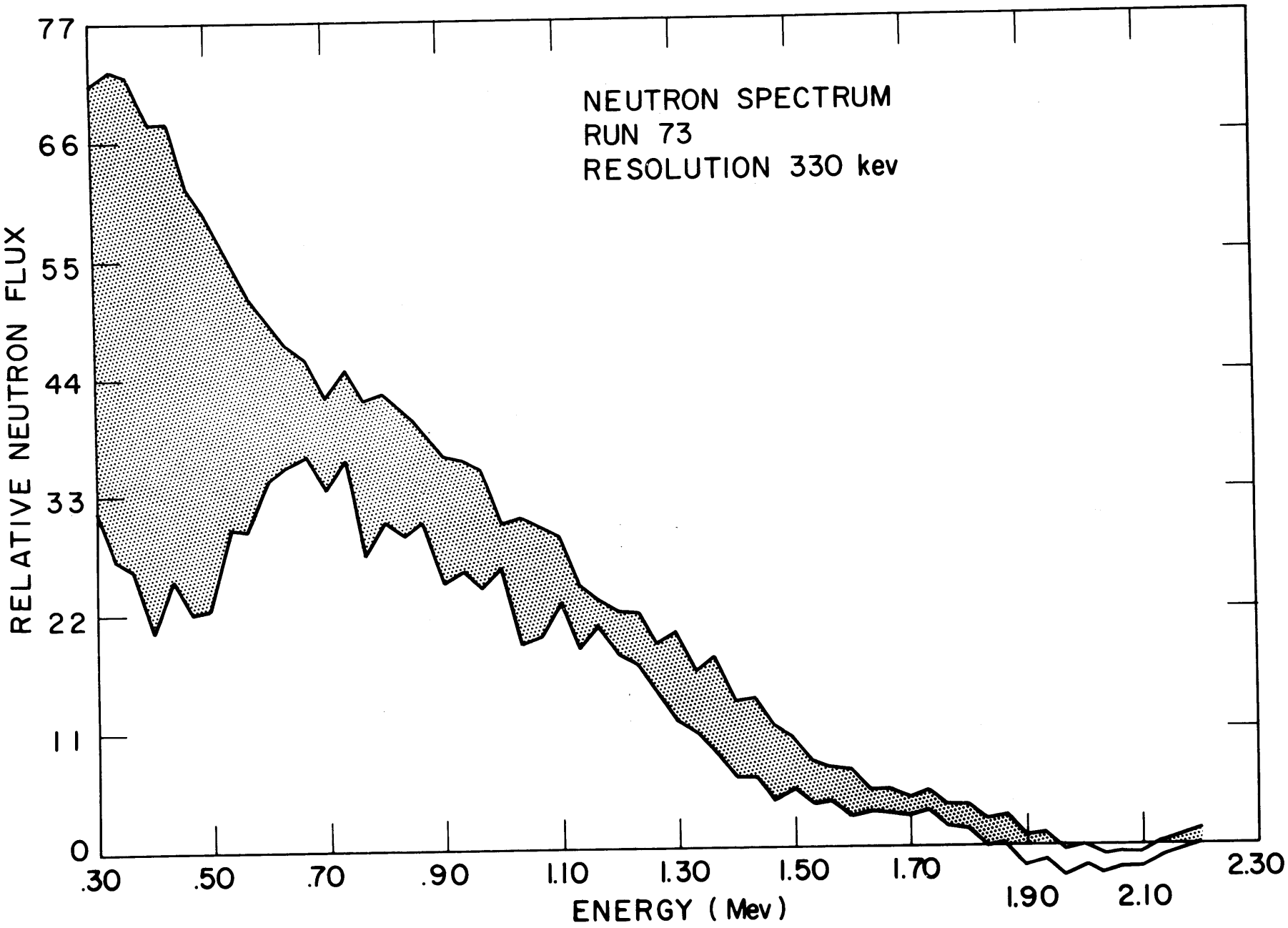
NEUTRON SPECTRUM
RUN 73
RESOLUTION 330 kev
RELATIVE NEUTRON FLUX
77
66
55
44
33
22
11
0
.30
.50
.70
.90
1.10
1.30
1.50
1.70
1.90
2.10
2.30
ENERGY (Mev)

figure 7_j

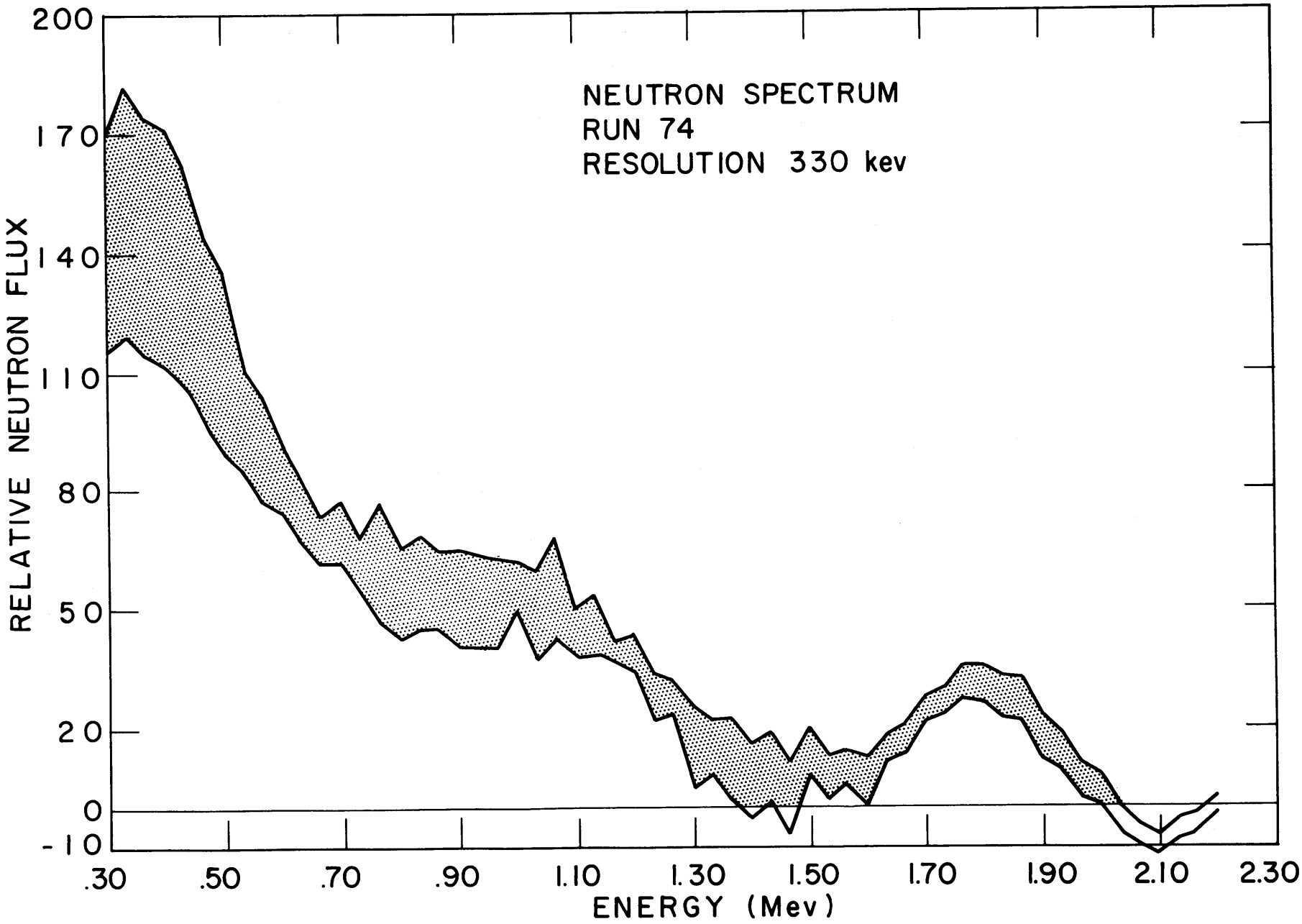
NEUTRON SPECTRUM
RUN 74
RESOLUTION 330 kev
RELATIVE NEUTRON FLUX
200
170
140
110
80
50
20
0
-10
.30
.50
.70
.90
1.10
1.30
1.50
1.70
1.90
2.10
2.30
ENERGY (Mev)

figure 7_k

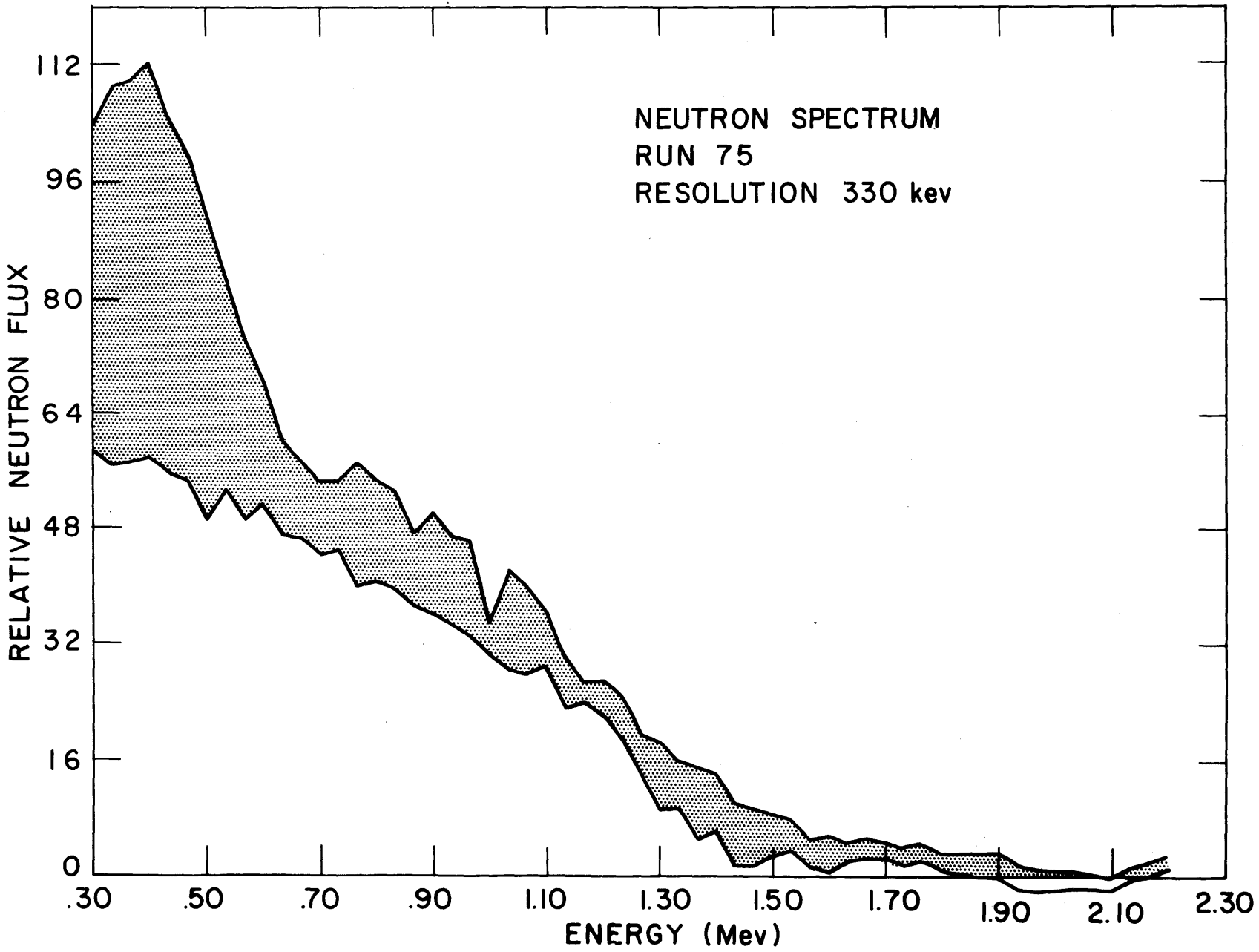
NEUTRON SPECTRUM
RUN 75
RESOLUTION 330 kev
RELATIVE NEUTRON FLUX
112
96
80
64
48
32
16
0
.30
.50
.70
.90
1.10
1.30
1.50
1.70
1.90
2.10
2.30
ENERGY (Mev)

figure 7_1

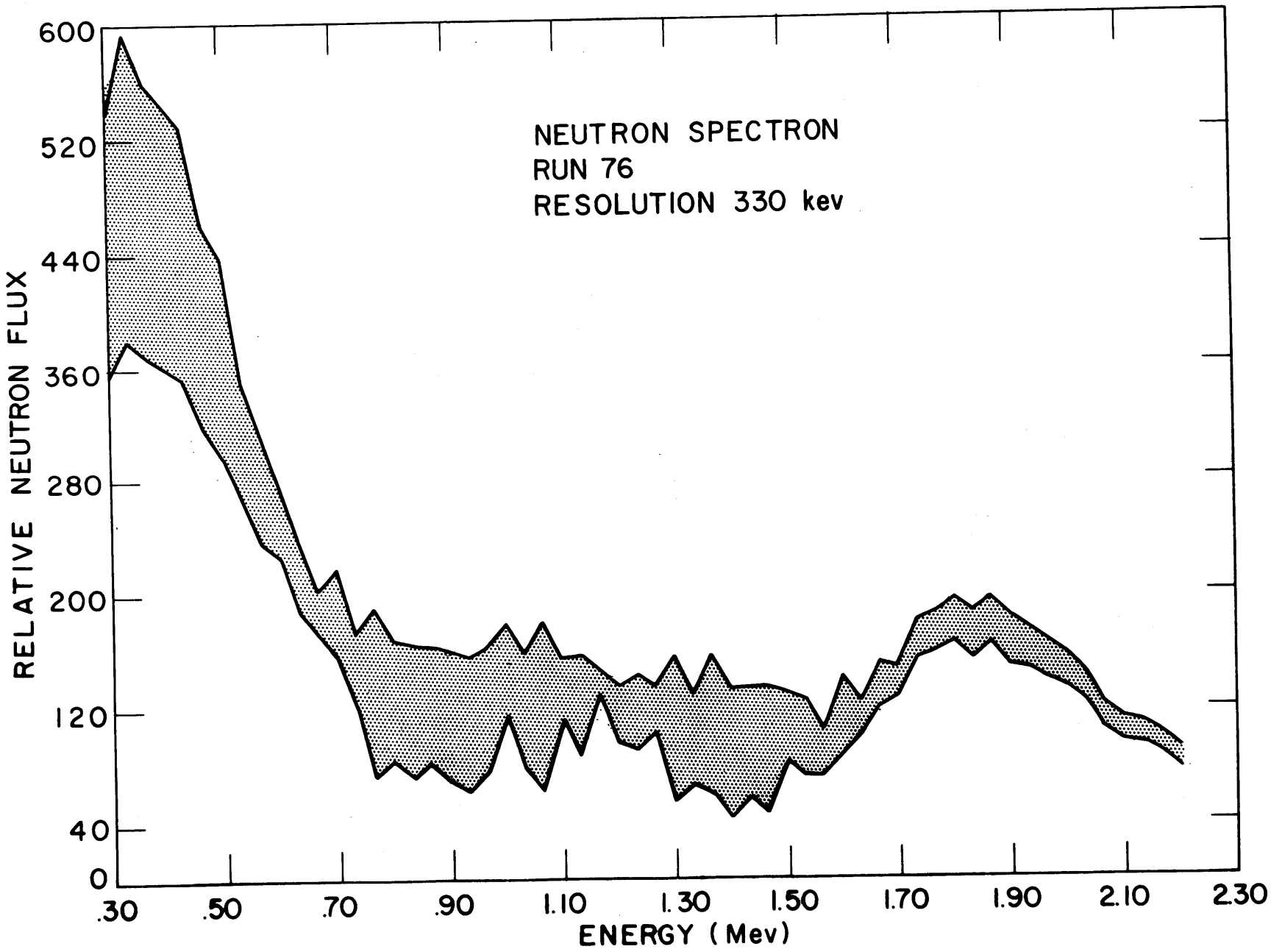
NEUTRON SPECTRON
RUN 76
RESOLUTION 330 kev
RELATIVE NEUTRON FLUX
600
520
440
360
280
200
120
40
0
.30
.50
.70
.90
1.10
1.30
1.50
1.70
1.90
2.10
2.30
ENERGY (Mev)

figure 7_m

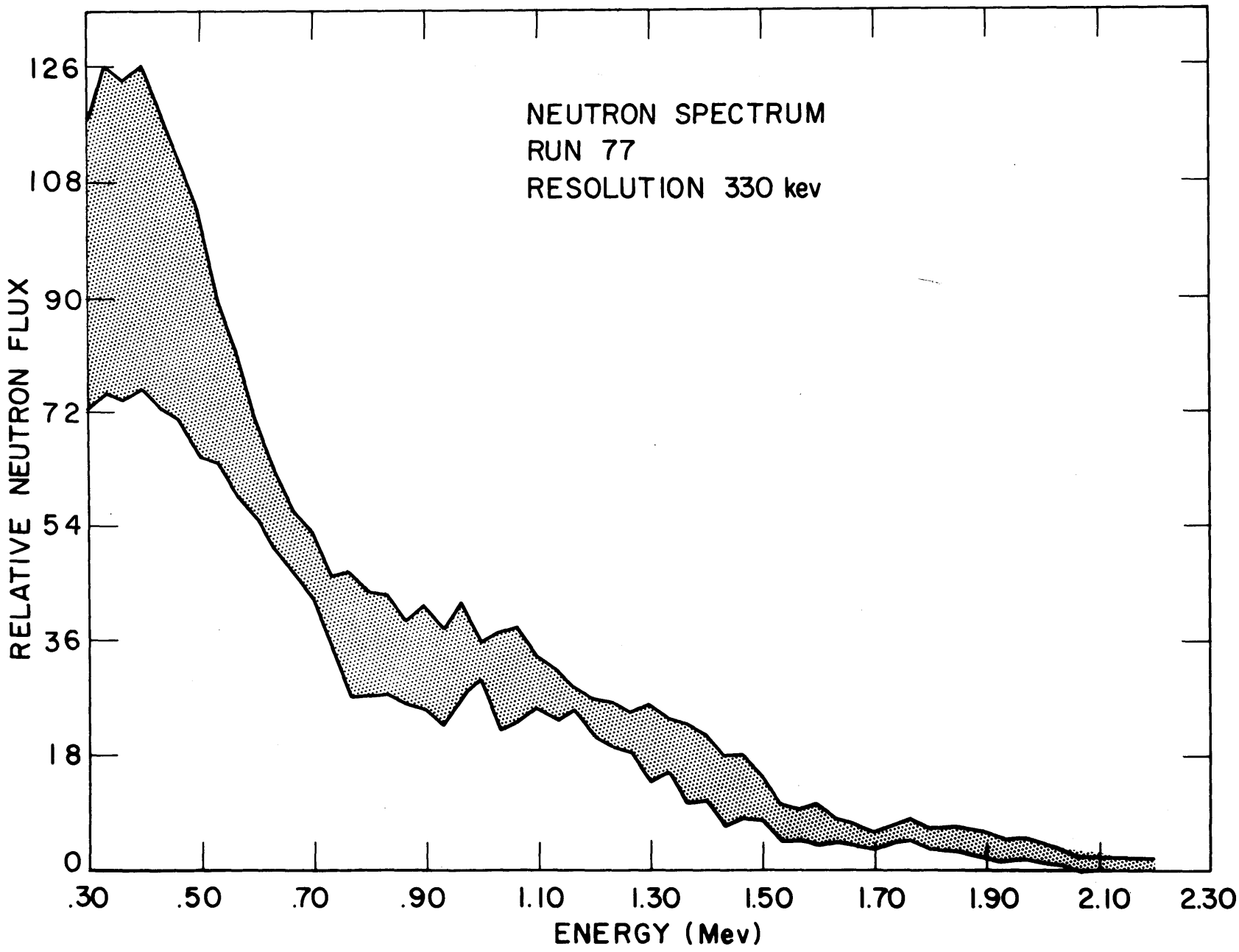
NEUTRON SPECTRUM
RUN 77
RESOLUTION 330 kev
RELATIVE NEUTRON FLUX
126
108
90
72
54
36
18
0
.30
.50
.70
.90
1.10
1.30
1.50
1.70
1.90
2.10
2.30
ENERGY (Mev)

figure 7_n

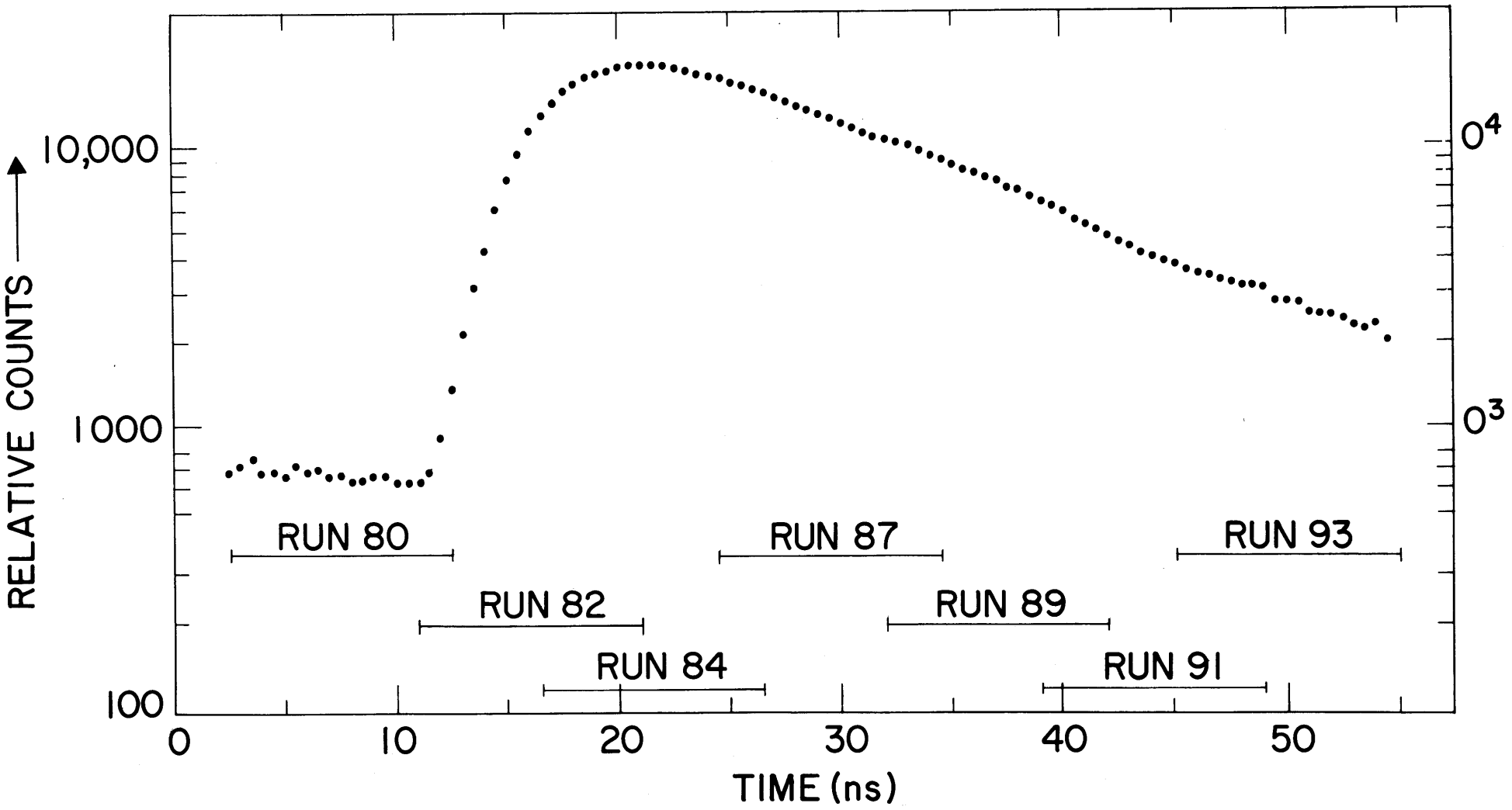

figure 8 - Time Spectrum from Iron Assembly

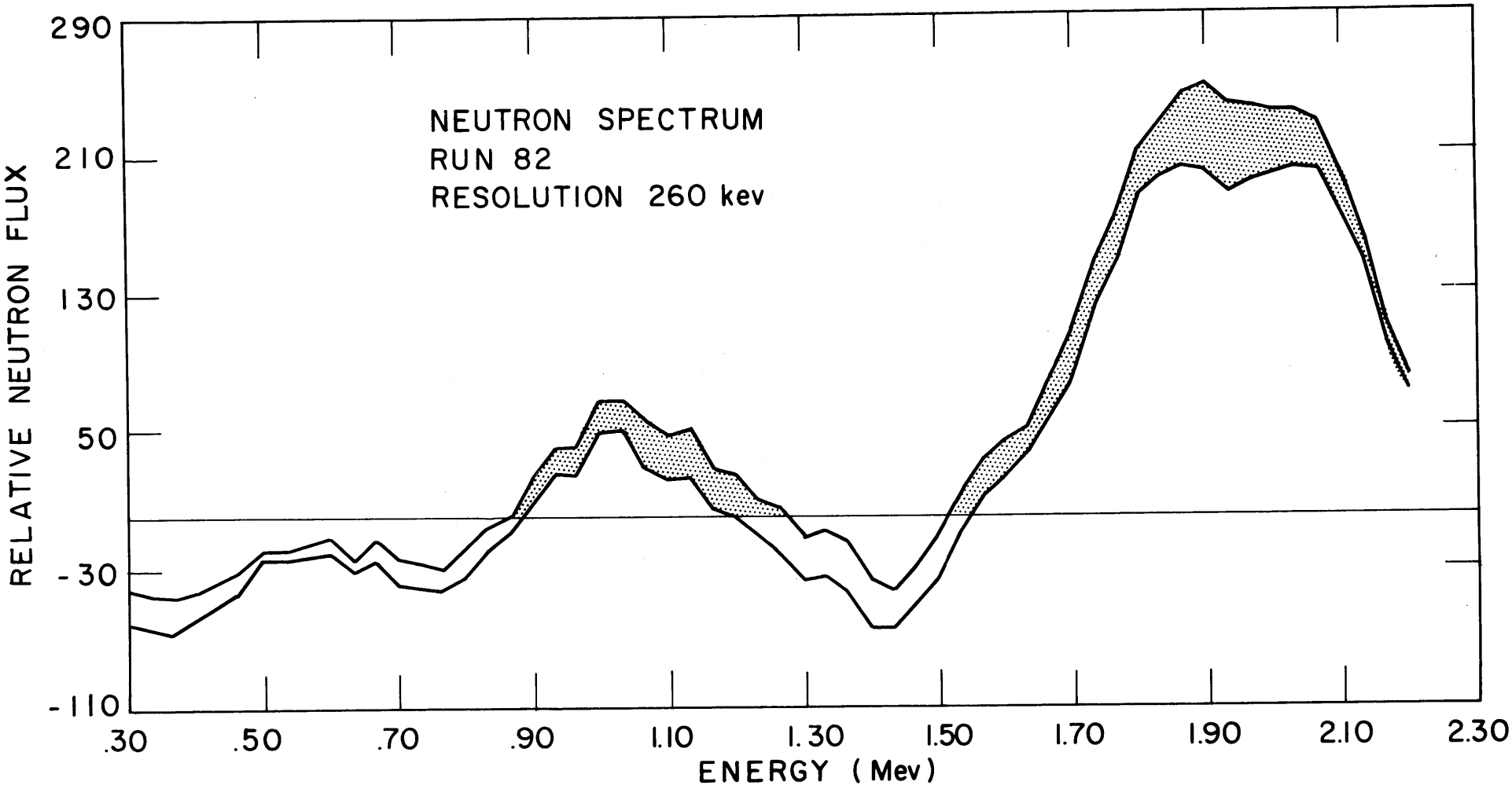
NEUTRON SPECTRUM
RUN 82
RESOLUTION 260 kev
RELATIVE NEUTRON FLUX
290
210
130
50
-30
-110
.30
.50
.70
.90
1.10
1.30
1.50
1.70
1.90
2.10
2.30
ENERGY (Mev)

figure 9_a

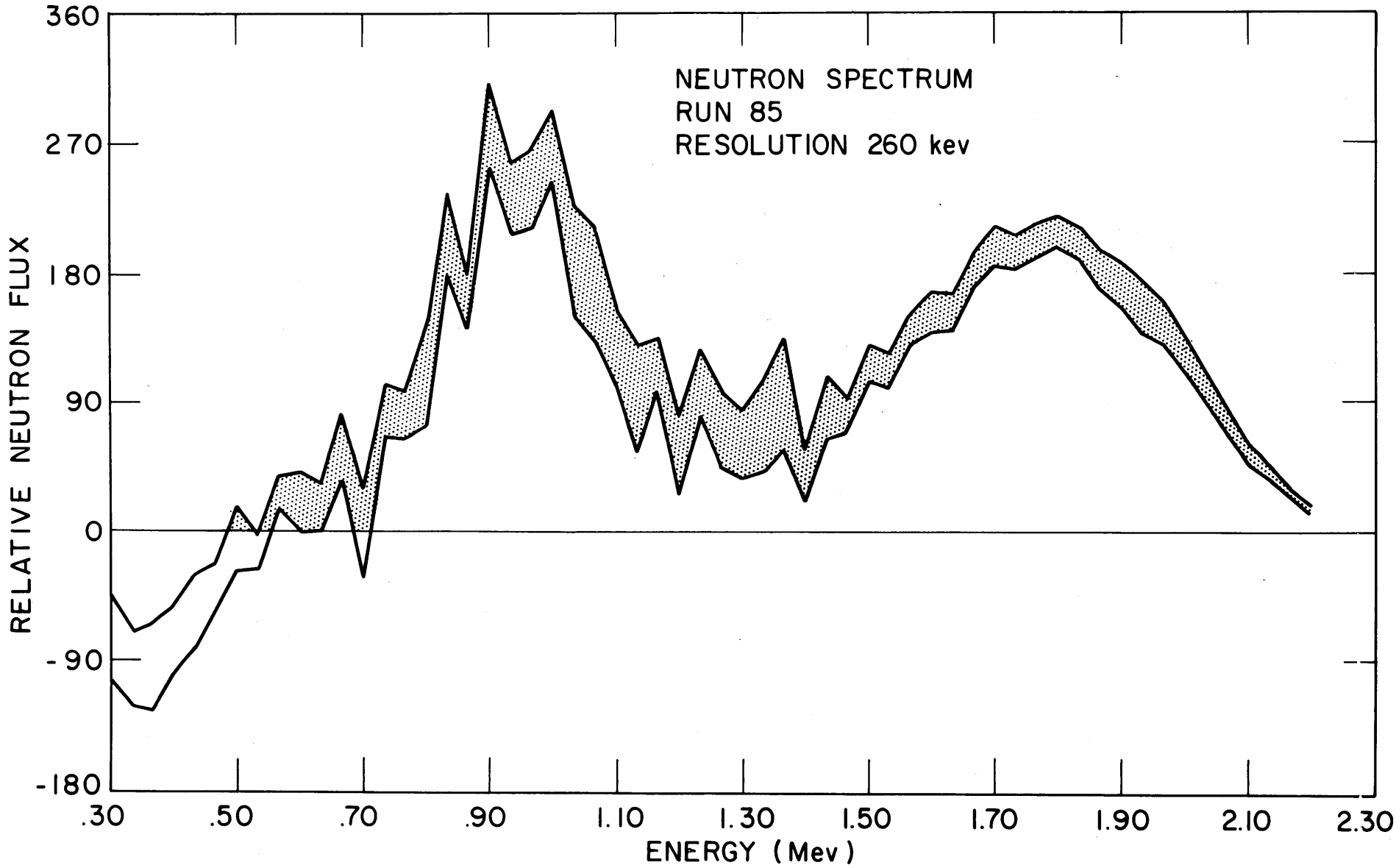
NEUTRON SPECTRUM
RUN 85
RESOLUTION 260 kev
RELATIVE NEUTRON FLUX
360
270
180
90
0
-90
-180
.30
.50
.70
.90
1.10
1.30
1.50
1.70
1.90
2.10
2.30
ENERGY (Mev)

figure 9_b

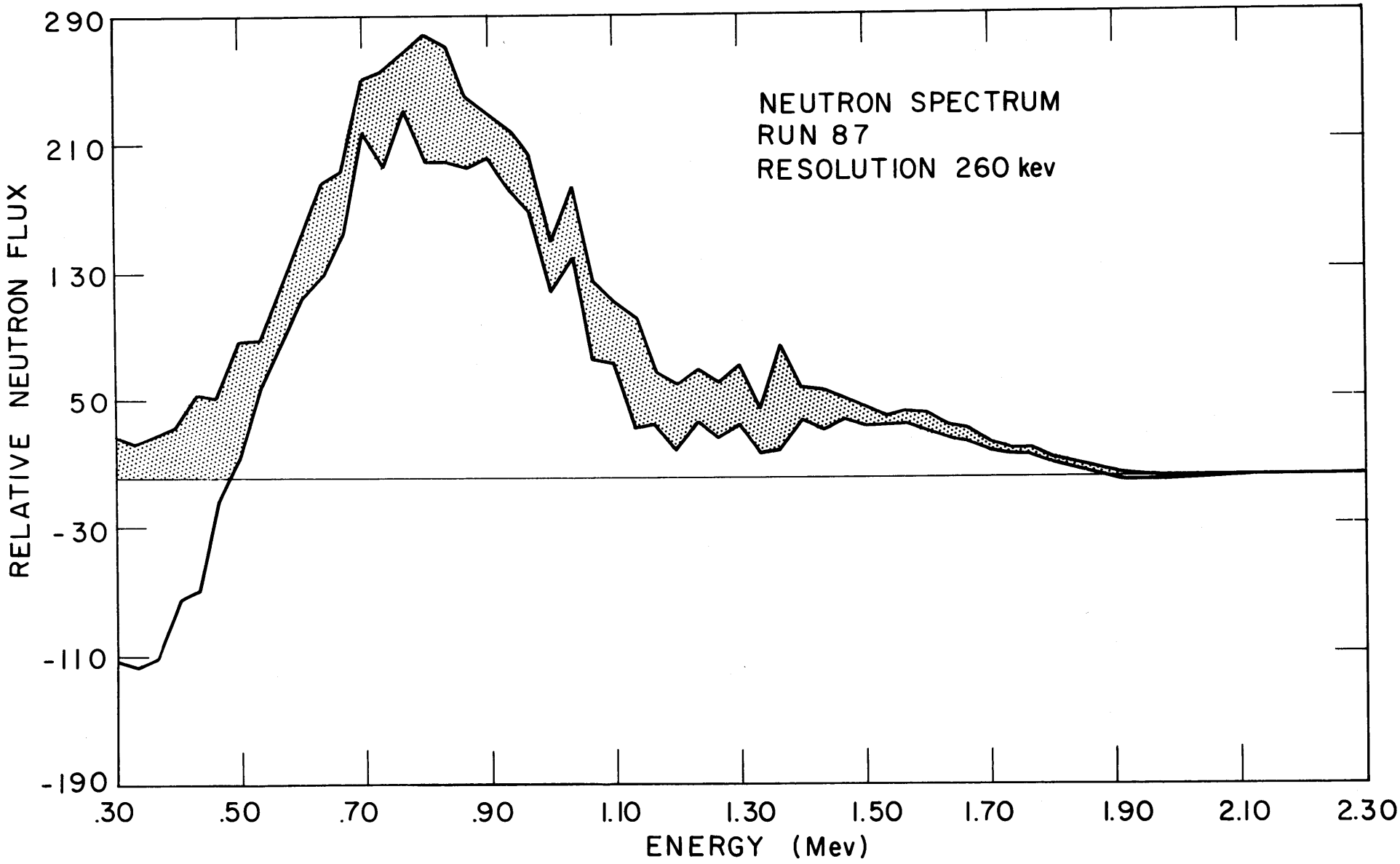
NEUTRON SPECTRUM
RUN 87
RESOLUTION 260 kev
RELATIVE NEUTRON FLUX
290
210
130
50
-30
-110
-190
.30
.50
.70
.90
1.10
1.30
1.50
1.70
1.90
2.10
2.30
ENERGY (Mev)

figure 9$_c$

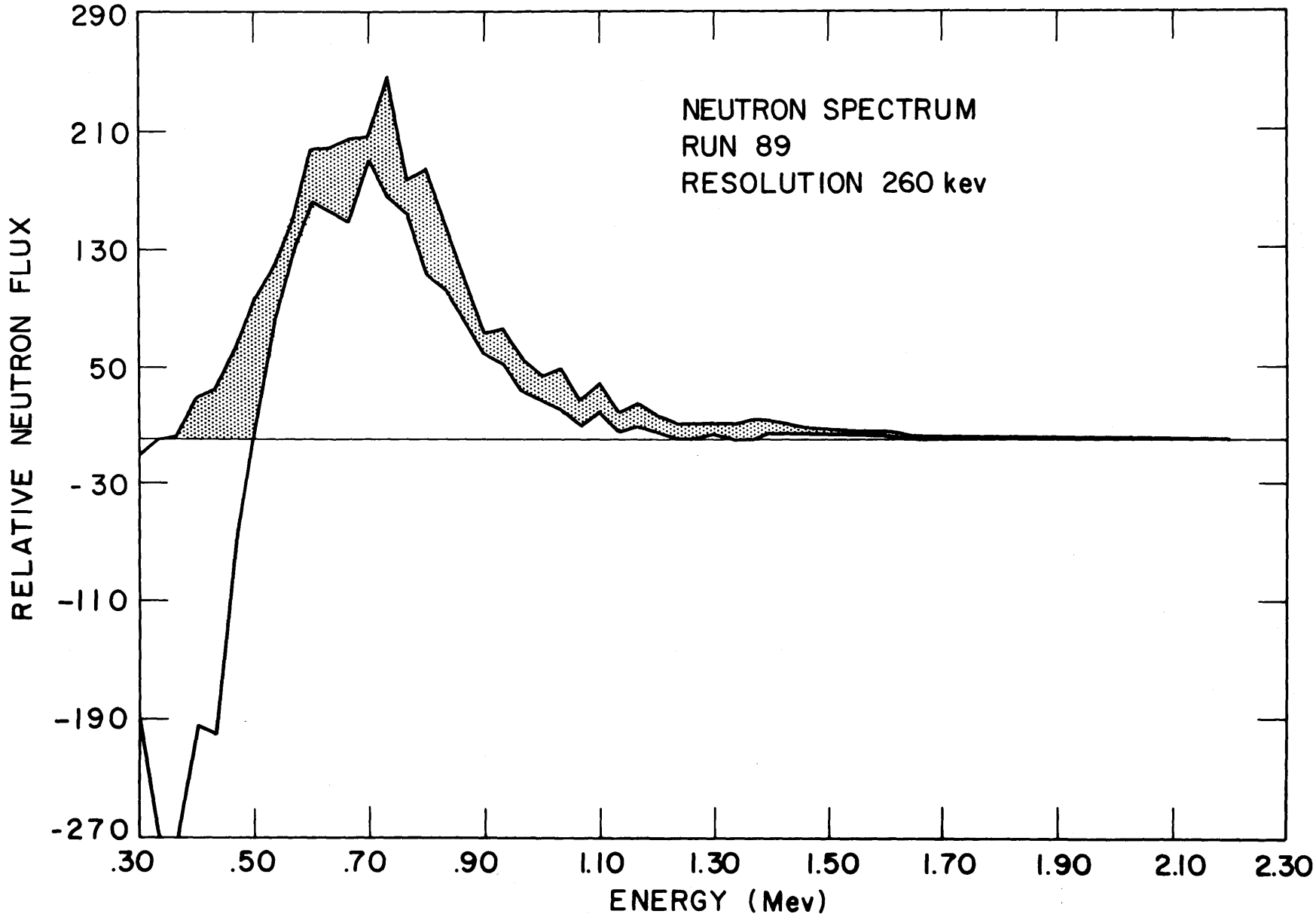
NEUTRON SPECTRUM
RUN 89
RESOLUTION 260 kev
RELATIVE NEUTRON FLUX
290
210
130
50
-30
-110
-190
-270
.30
.50
.70
.90
1.10
1.30
1.50
1.70
1.90
2.10
2.30
ENERGY (Mev)

figure 9_d

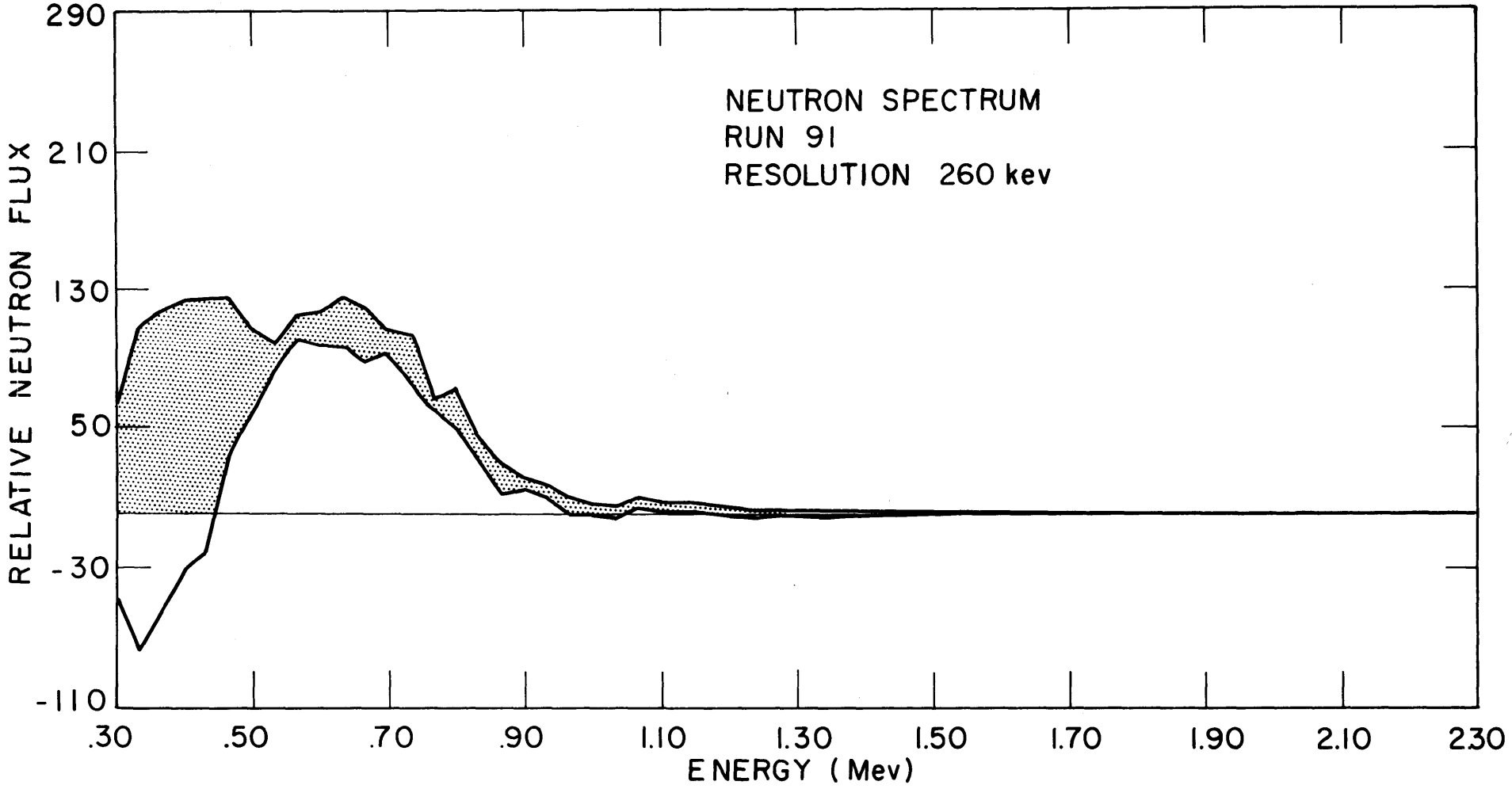
NEUTRON SPECTRUM
RUN 91
RESOLUTION 260 kev
RELATIVE NEUTRON FLUX
290
210
130
50
-30
-110
.30
.50
.70
.90
1.10
1.30
1.50
1.70
1.90
2.10
230
ENERGY (Mev)

figure 9_e

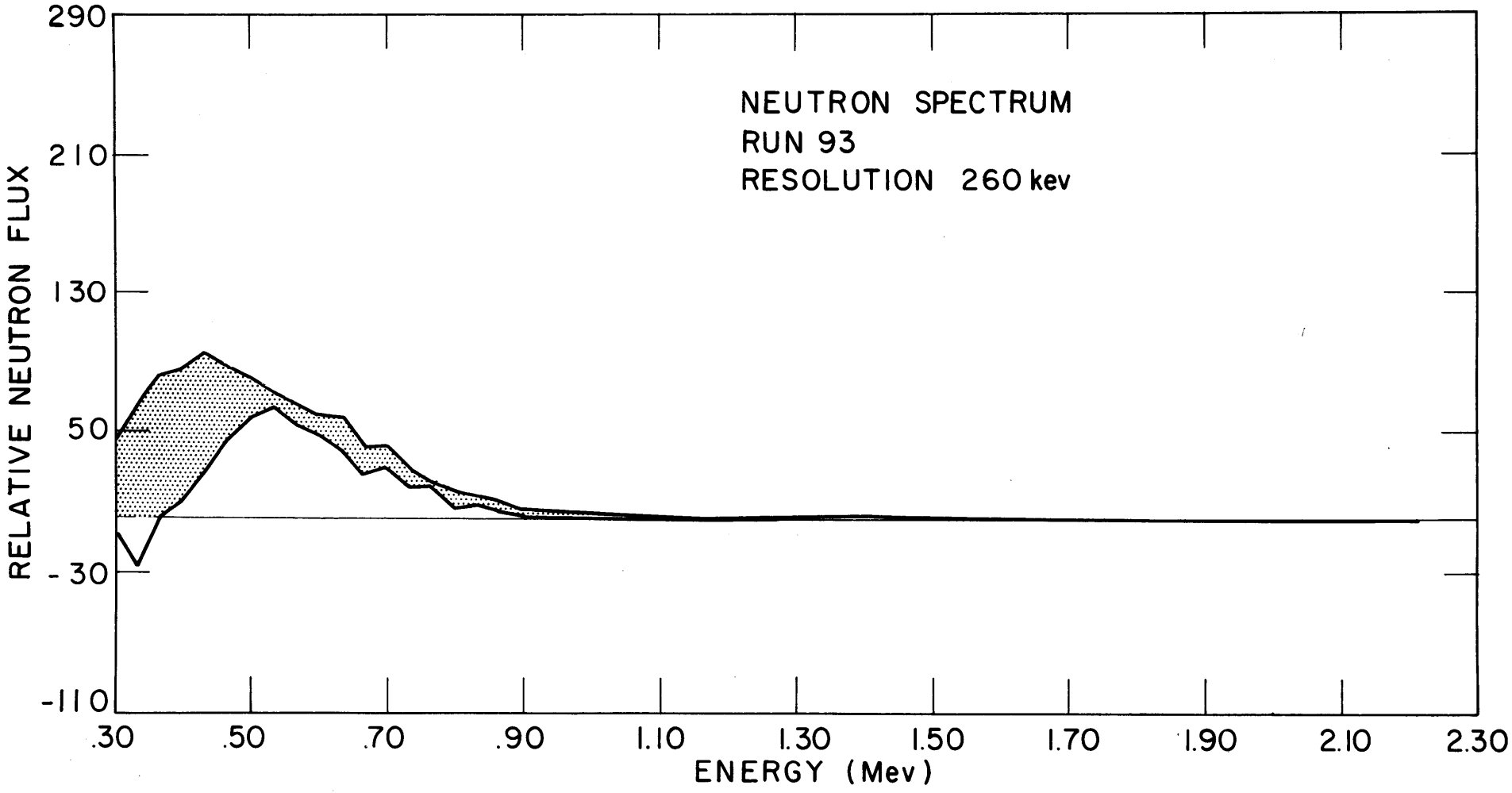
NEUTRON SPECTRUM
RUN 93
RESOLUTION 260 kev
RELATIVE NEUTRON FLUX
290
210
130
50
- 30
-110
.30
.50
.70
.90
1.10
1.30
1.50
1.70
1.90
2.10
2.30
ENERGY (Mev)

figure 9_f